

New Measurements of the Ionizing Ultraviolet Background over $2 < z < 5$ and Implications for Hydrogen Reionization

George D. Becker^{1*} & James S. Bolton²

¹*Kavli Institute for Cosmology and Institute of Astronomy, University of Cambridge, Madingley Rd, Cambridge, CB3 0HA, UK*

²*School of Physics and Astronomy, University of Nottingham, University Park, Nottingham NG7 2RD*

Draft version 29 October 2018

ABSTRACT

We present new measurements of the intensity of the ionizing ultraviolet background and the global emissivity of ionizing photons over $2 < z < 5$. Our results are based on a suite of updated measurements of physical properties of the high-redshift intergalactic medium (IGM), including gas temperatures and the opacity of the IGM to Ly α and ionizing photons. Consistent with previous works, we find a relatively flat hydrogen photoionization rate over $2 < z < 5$, although our measurements are roughly a factor of two higher than the 2008 values of Faucher-Giguère et al., due primarily to our lower gas temperatures. The ionizing emissivity we derive is also generally higher than other recent estimates due to a combination of lower gas temperatures, higher ionizing opacity, and an accounting of cosmological radiative transfer effects. We find evidence that the emissivity increases from $z \sim 3$ to 5, reaching ~ 5 ionizing photons per atom per gigayear at $z = 4.75$ for realistic galaxy spectra. We further find that galaxies must dominate the emissivity near 1 Ryd at $z \geq 4$, and possibly at all redshifts $z \geq 2.4$. Our results suggest that the globally-averaged ionizing “efficiency” of star-forming galaxies increases substantially with redshift over $3.2 \leq z \leq 4.75$. This trend is consistent with the conclusion often drawn from reionization models that the ionizing efficiency of galaxies must be higher during reionization in order for galaxies to reionize the IGM by $z = 6$. Our emissivity values at $z \sim 5$ suggest that ionizing photons may have been a factor of two more abundant during the final stages of reionization than previously indicated. The evolution of the ionizing emissivity over $2 < z < 5$ suggests, moreover, that the steep decline in the photoionization rate from $z \sim 5$ to 6 may indicate a rapid evolution in the mean free path at $z > 5$.

Key words: intergalactic medium - quasars: absorption lines - reionization - cosmic background radiation - cosmology: observations - large-scale structure of the Universe - galaxies: high-redshift

1 INTRODUCTION

The ionizing ultraviolet background (UVB) is a key probe of the interaction between luminous sources and the intergalactic medium (IGM). Following hydrogen reionization, the nearly complete ionization of the IGM is maintained by ultraviolet photons from star-forming galaxies and active galactic nuclei (AGN). Many (or most) of these sources are too faint, however, to observe directly at high redshifts. Moreover, the ionizing portions of their spectra are largely obscured due to absorption from the IGM. Measurements of the UVB derived from the properties of the IGM itself therefore provide unique insights into critical aspects

of galaxy and AGN evolution that are difficult to study by other means.

Studies of the UVB have particular relevance for understanding how and when the IGM became reionized. For example, the properties of the UVB following reionization provide a boundary condition on the evolution of the ionizing radiation field during reionization itself. The intensity of the UVB at $z \sim 5 - 6$, in particular, can help to determine how abundant ionizing photons in the IGM may have been during the final stages of reionization. Previous measurements of a low ionizing emissivity at these redshifts suggested that reionization may have been a “photon-starved” process, with only $\sim 2-3$ ionizing photons being emitted per baryon per gigayear at $z = 6$ (Miralda-Escudé 2003; Meiksin

* gdb@ast.cam.ac.uk

2005; Bolton & Haehnelt 2007; Kuhlen & Faucher-Giguère 2012).

The redshift evolution of the UVB can also help to identify trends that clarify how galaxies and/or AGN were able to produce and emit enough ionizing photons to reionize the IGM by $z = 6$ (Fan et al. 2006). Direct searches for star-forming galaxies at $z > 6$ indicate that the global star formation rate density declines steeply with redshift over $6 < z < 12$ (e.g., Ouchi et al. 2009; Castellano et al. 2010; Bunker et al. 2010; Bouwens et al. 2006, 2008, 2011, 2012; Oesch et al. 2010; McLure et al. 2010, 2013; Schenker et al. 2013; Ellis et al. 2013). Even when accounting for sources below the detection limits, reionization models based on the measured non-ionizing UV galaxy luminosity functions typically require that reionization-era galaxies emit significantly more ionizing photons, relative to their non-ionizing luminosity, than their lower-redshift counterparts (e.g., Ouchi et al. 2009; Kuhlen & Faucher-Giguère 2012; Mitra et al. 2013; Robertson et al. 2013; Ferrara & Loeb 2013). This ionizing “efficiency” is often parametrized in terms of the relative escape fraction of ionizing photons, but also depends on a galaxy’s intrinsic UV spectral energy distribution.

Direct searches for ionizing emission from star-forming galaxies suggests that typical ionizing escape fractions (and/or intrinsic ratios of ionizing to non-ionizing luminosity) may indeed be larger at earlier times. Siana et al. (2010), for example, find $f_{\text{esc}} < 0.04$ at $z \sim 1$, while Nestor et al. (2013) find $f_{\text{esc}} \sim 5 - 7$ per cent for Lyman break galaxies (LBGs) and $f_{\text{esc}} \sim 10 - 30$ per cent for fainter Lyman-alpha emitters (LAEs) (see also Mostardi et al. 2013). Although directly detecting the ionizing flux from galaxies becomes extremely difficult at $z \geq 4$, indirect evidence that the escape fraction may continue increasing with redshift at $z > 3$ comes from an observed increase with redshift in the fraction of LBGs showing Ly α emission (Stark et al. 2010, 2011) combined with an anticorrelation between Ly α fraction and the covering fraction of H I gas (Jones et al. 2012).

Measurements of the UVB can help clarify these trends by providing a census of the ionizing emissivity from all sources, a quantity that is essentially impossible to obtain from direct observations alone. The ionizing emissivity can then be compared to the non-ionizing UV emissivity measured directly from galaxies and AGN in order to assess the evolution in ionizing efficiency.

In this paper we present new calculations of the H I photoionization rate and the ionizing emissivity over $2 < z < 5$. Our results are based on multiple recent measurements of the physical properties of the high-redshift IGM, including gas temperatures and the mean opacity of the IGM to Ly α and ionizing photons. Our work builds upon previous measurements of the UVB using the mean Ly α opacity (e.g., Rauch et al. 1997; Songaila et al. 1999; McDonald & Miralda-Escudé 2001; Meiksin & White 2003; Tytler et al. 2004; Jena et al. 2005; Kirkman et al. 2005; Bolton et al. 2005; Fan et al. 2006; Bolton & Haehnelt 2007; Faucher-Giguère et al. 2008a; Wyithe & Bolton 2011; Kuhlen & Faucher-Giguère 2012) and the quasar proximity effect (e.g., Bajtlik et al. 1988; Scott et al. 2000; Dall’Aglio et al. 2008; Calverley et al. 2011). The new measurements of the IGM properties are significantly more pre-

cise than previous estimates, and allow us to conduct a detailed examination of the evolution of the UVB in the post-reionization epoch. A key advantage of the present work is the fact that we have self-consistent measurements of the temperature, Ly α opacity, and ionizing opacity extending over $2 < z < 5$, allowing us to study the evolution of the UVB over a wide redshift range and as close as possible to the reionization epoch itself.

In Section 2 we briefly describe the IGM measurements upon which our analysis is based. The hydrodynamical simulations used to calibrate these measurements are described in Section 3. In Section 4 we present our results for the H I photoionization rate, which are derived from the Ly α opacity and gas temperature of the IGM. In Section 5 we combine these results with measurements of the opacity of the IGM to ionizing photons to derive the ionizing emissivity. We then turn towards disentangling the contribution to the emissivity from AGN and galaxies in Section 6, and compare our results for the integrated ionizing emissivity from galaxies to the non-ionizing UV emissivity measured from galaxy surveys. We then discuss the implications of our results for the evolution of the ionizing efficiency of galaxies and for hydrogen reionization in Section 7 before concluding in Section 8. Our results assume a flat Λ CDM cosmology with $\Omega_{\text{m}} = 0.308$, $\Omega_{\Lambda} = 0.692$, $\Omega_{\text{b}}h^2 = 0.0222$, $h = 0.678$, $\sigma_8 = 0.829$, and $n_s = 0.961$, consistent with recent *Planck*+WP+highL+BAO constraints from Planck Collaboration XVI (2013), although uncertainties in the cosmological parameters are also taken into account.

2 THE DATA

Our analysis of the UV background draws on multiple recent measurements of physical properties of the high-redshift IGM. Here we briefly describe these measurements, while in Sections 4 and 5 we detail how they are used to calculate the hydrogen photoionization rate and the ionizing emissivity.

The calculations of the hydrogen photoionization rate, Γ , are based on the mean opacity of the IGM to Ly α photons and the temperature of the IGM. The Ly α opacity is quantified in terms of an effective optical depth, $\tau_{\text{eff}}^{\alpha} = -\ln \langle F \rangle$, where F is the continuum-normalized transmitted flux in the Ly α forest. Measurements of $\tau_{\text{eff}}^{\alpha}$ over $2.15 \leq z \leq 4.85$ are taken from Becker et al. (2013). This work used composites of quasar spectra drawn from the Sloan Digital Sky Survey (York et al. 2000) to perform a differential measurements of the mean transmitted Ly α flux as a function of redshift, normalizing the results to measurements at $z \leq 2.5$ made from high-resolution data by Faucher-Giguère et al. (2008b). This approach has the advantage of avoiding the need to continuum-fit individual spectra at high redshifts, where the Ly α forest becomes heavily absorbed, enabling a precise measurement of $\tau_{\text{eff}}^{\alpha}$ up to $z \sim 5$.

Our temperature measurements are taken from Becker et al. (2011), who used the curvature of the Ly α forest in a large set of high-resolution quasar spectra to determine IGM temperatures over $2.0 \leq z \leq 4.8$. At a given redshift, they measured only the temperature at an optimal overdensity probed by the forest, $T(\bar{\Delta})$, where the temperature at that density, as determined from the curvature, did

not depend on the overall shape of the temperature-density relation. This approach provides an accurate measurement of the temperature at a single density, but does not constrain the overall shape of the temperature-density relation. We therefore quantify systematic uncertainties in our estimate of the ionization rate related to the shape of the temperature-density relation in Section 4. The error bars reported by Becker et al. (2011) are statistical only; however, they also note a systematic uncertainty related to the integrated thermal history. To account for this, we add 2000 K to the errors in $T(\bar{\Delta})$ at each redshift, which is close to the typical systematic error.

Translating our values for the ionization rate into estimates of the ionizing emissivity requires quantifying the opacity of the IGM (and circum-galactic medium; CGM) to ionizing photons. For this we combine two sets of recent measurements. The first is a set of direct determinations of the mean free path for 1 Ryd photons, λ_{912} , over $2.4 \leq z \leq 4.9$ derived from composite quasar spectra (Prochaska et al. 2009; O’Meara et al. 2013; Fumagalli et al. 2013, Worseck et al., in prep). This method has the advantage that it directly probes the combined IGM+ICM opacity without needing to know the detailed H I column density distribution. As described in the appendix, however, a correct calculation of the emissivity at $z \simeq 2-3$, where the mean free path is substantial, requires quantifying the opacity to ionizing photons as a function of frequency and redshift. We do this by combining the direct measurements of λ_{912} with measurements of the incidence rate of optically-thick Lyman limit systems (LLSs) over $2.7 \leq z \leq 4.4$ from Songaila & Cowie (2010). As described in Section 5, the n_{LLS} measurements are not used to refine the measurement of λ_{912} , but rather to approximately constrain the shape of the H I column density distribution over the column density range that dominates the ionizing opacity. This then enables us to calculate the IGM+CGM opacity as a function of frequency and redshift.

3 HYDRODYNAMICAL SIMULATIONS

We use hydrodynamical simulations of the IGM to calibrate our measurements of the H I ionization rate. The simulations used here build on the runs described in Becker et al. (2011) and are performed with the cosmological hydrodynamical code GADGET-3, an updated version of the publicly available code GADGET-2 (Springel 2005). Briefly, our primary simulations are performed in a $10h^{-1}$ comoving Mpc box with a gas particle mass of $9.2 \times 10^4 h^{-1} M_{\odot}$. The simulations explore a wide range of IGM thermal histories which are summarized in Table 2 of Becker et al. (2011). In this work, we supplement these simulations with several additional runs which we now turn to describe briefly here.

The fiducial cosmology assumed in our simulations consists of a flat Λ CDM cosmology with $\Omega_{\text{m}} = 0.26$, $\Omega_{\Lambda} = 0.74$, $\Omega_{\text{b}} h^2 = 0.023$, $h = 0.72$, $\sigma_8 = 0.80$, and $n_{\text{s}} = 0.96$. As discussed in Bolton et al. (2005) and Bolton & Haehnelt (2007), however, the calibration of H I ionization rate as a function of Ly α opacity will depend on cosmology. We therefore performed an addition run, C15_P, with the same thermal history as run C15 in Becker et al. (2011) but using $\Omega_{\text{m}} = 0.308$, $\Omega_{\Lambda} = 0.692$, $\Omega_{\text{b}} h^2 = 0.0222$, $h = 0.678$, $\sigma_8 = 0.829$, and $n_{\text{s}} = 0.961$, consis-

tent with the *Planck*+WP+highL+BAO constraints from Planck Collaboration XVI (2013). Corrections to Γ for cosmology as a function of redshift were then computed by comparing the results obtained using run C15 and C15_P. The result was a 14 to 19 per cent reduction in Γ when using the *Planck* cosmology, a similar but somewhat smaller correction than that computed from the scaling relations for individual cosmological parameters derived in Bolton et al. (2005) and Bolton & Haehnelt (2007).

Convergence of Γ with box size and mass resolution were checked using the ‘‘R’’ runs from Becker et al. (2011), in which we alternately varied the mass resolution and box size. The results indicated that we are well converged with mass resolution at our nominal value of $M_{\text{gas}} = 9.2 \times 10^4 h^{-1} M_{\odot}$, with at most a 2 per cent increase in Γ when using a factor of eight coarser resolution (run R1). We did find, however, that the results using our nominal box size of $10 h^{-1}$ Mpc over-predicted Γ by roughly 10 percent compared to those using the $40 h^{-1}$ Mpc box (run R4). This is presumably due to the fact that the smaller box contains fewer rare, deep voids, which tend to decrease the mean Ly α opacity. We therefore applied a redshift-dependent box size correction, finding that $\Gamma^{40}/\Gamma^{10} = 0.90 - 0.018z + 0.0041z^2$ provided a good fit over $2 < z < 5$. Our convergence results are consistent with those presented by Bolton & Becker (2009).

Our fiducial results were calculated using the density and peculiar velocity fields from a simulation in which hydrogen reionization begins at $z = 12$ and is initially heated to a maximum temperature of $\sim 9,000$ K by $z \simeq 9$ (see Figure B1). Different thermal histories will alter the small-scale density field and peculiar velocity fields via Jeans smoothing, which can potentially impact the mean Ly α opacity. As described in Appendix B, however, these effects were tested and found to have a minimal impact on our results.

4 H I IONIZATION RATE

4.1 Method

The intensity of the ionizing ultraviolet background is typically characterized by either the specific intensity at the Lyman limit, J_{912} , or the total hydrogen ionization rate, Γ . These quantities are related as

$$\Gamma(z) = 4\pi \int_{\nu_{912}}^{\infty} \frac{d\nu}{h\nu} J_{\nu}(z) \sigma_{\text{HI}}(\nu), \quad (1)$$

where $\sigma_{\text{HI}}(\nu)$ is the photoionization cross section. Since the shape of the ionizing background is not known a priori, the photoionization rate is a more model-independent measure of the intensity of the UVB. Within the context of a given cosmological model, Γ can be derived from the opacity of the IGM to Ly α photons, provided the gas temperature is also known. In photoionization equilibrium, the local optical depth of the IGM to Ly α scattering (Gunn & Peterson 1965), neglecting the effects of peculiar velocities and thermal broadening, is given by (e.g., McDonald & Miralda-Escudé 2001)

$$\tau \propto \frac{(1+z)^6 (\Omega_{\text{b}} h^2)^2}{T^{0.7} H(z) \Gamma(z)} \Delta^{\beta}, \quad (2)$$

where $\Delta = \rho/\langle\rho\rangle$ is the fractional overdensity. The temperature scaling here reflects the temperature dependence of the

recombination rate. For a power law temperature-density relation of the form $T(\Delta) = \bar{T}(\Delta/\bar{\Delta})^{\gamma-1}$, the slope with density is given by $\beta = 2 - 0.7(\gamma - 1)$.

To predict $\tau_{\text{eff}}^{\alpha}$ as a function of Γ , the local optical depths must be integrated over a realistic density distribution, and both peculiar velocities and thermal broadening must be taken into account. To do this, we follow Bolton et al. (2005) and Bolton & Haehnelt (2007) in calibrating our Γ results using artificial Ly α forest spectra drawn from hydrodynamical simulations. The simulated spectra are used to predict $\tau_{\text{eff}}^{\alpha}$ for a given ionization rate and temperature-density relation. We thus measure Γ at a given redshift by matching the temperatures in the simulation to our observed values and tuning the ionization rate such that the predicted $\tau_{\text{eff}}^{\alpha}$ matches the observed value (e.g., Theuns et al. 1998).

The effective optical depths from Becker et al. (2013) consist of twenty-eight $\tau_{\text{eff}}^{\alpha}$ values over $2.15 \leq z_{\alpha} \leq 4.85$ in bins of $\Delta z_{\alpha} = 0.1$, while the temperature measurements consist of eight $T(\bar{\Delta})$ measurements over $2.0 < z_{\text{T}} < 4.8$ in bins of $\Delta z_{\text{T}} = 0.4$. Our approach for determining the best-fitting values of $\Gamma(z)$ attempts to make optimal use of these data while accounting for the fact they have different redshift binnings.

We first determine the best-fitting values of Γ for each $\tau_{\text{eff}}^{\alpha}$ measurement using the $T(\bar{\Delta})$ value linearly interpolated onto redshift z_{α} and a fixed value for γ . For each z_{α} we identify the four nearest simulation output redshifts, two at $z_{\text{sim}} < z_{\alpha}$ and two at $z_{\text{sim}} > z_{\alpha}$. Using the optical depths along 1000 random lines of sight generated from the native temperature, density, and velocity fields of the fiducial simulation, we determine the ionization rate needed to reproduce the observed effective optical depth at each of the four simulation redshifts. We adjust these Γ values to the interpolated value of $T(\bar{\Delta})$ and chosen value of γ using the scaling relations described in Appendix A. The best-fitting value for Γ at z_{α} is then determined using a power law fit to Γ versus $1 + z_{\text{sim}}$. Cosmology and box size corrections are applied. Finally, in order to minimize the correlation introduced by interpolating the temperatures, we average the Γ results over the temperature redshift bins. There are four $\tau_{\text{eff}}^{\alpha}$ measurements per temperature bin for all except the highest-redshift point, for which there are three.

Statistical errors for Γ are calculated using a Monte Carlo approach in which the values of $\tau_{\text{eff}}^{\alpha}$ and $T(\bar{\Delta})$ are varied randomly. Realizations for $\tau_{\text{eff}}^{\alpha}$ were drawn using the full covariance matrix given by Becker et al. (2013). We also propagate errors in the cosmological parameters through to our Γ results by generating random sets of cosmological parameters from the full *Planck* posterior distributions. The corresponding errors in Γ are then estimated using the scaling relations in Bolton et al. (2005) and Bolton & Haehnelt (2007).

The temperature measurements of Becker et al. (2011) specify the temperature at a specific overdensity at which $T(\bar{\Delta})$ could be determined independently from the shape of the temperature-density relation, and do not provide constraints on γ . We therefore evaluate Γ over a range in γ that attempts to bracket the likely values at these redshifts. In photoionization equilibrium, γ is expected to asymptotically reach a maximum value of $\gamma \simeq 1.6$ (Hui & Gnedin 1997), which we take as an upper limit. For our minimum value we adopt $\gamma = 1.2$, which corresponds to a significantly flat-

tened temperature-density relation. For simplicity, we adopt $\gamma = 1.4$ as our fiducial value.

In principle γ can be lower than 1.2, with the temperature-density relation becoming flat or even inverted ($\gamma < 1$) immediately following a reionization event. After reionization, however, the voids are expected to cool rapidly via adiabatic expansion, driving γ towards its asymptotic value. Simulations of hydrogen reionization suggest that γ should only be less than 1.2 near $z \sim 5$, and then only if a majority of the voids are reionized close to $z = 6$ (e.g., Trac et al. 2008; Furlanetto & Oh 2009), a scenario currently disfavored by observations of $z = 6.6$ Ly α -emitting galaxies (e.g., Ouchi et al. 2010). In a patchy and extended helium reionization (e.g., Becker et al. 2011), the globally-averaged temperature-density relation is also unlikely to flatten dramatically (McQuinn et al. 2009; Compostella et al. 2013), although it may be flat or inverted locally. We note that some analyses of the Ly α flux probability distribution function have yielded tentative evidence of a flat or inverted temperature-density relation near $z \sim 2 - 3$ (e.g., Bolton et al. 2008; Viel et al. 2009), although it has been argued these measurements are sensitive to systematic effects such as quasar continuum placement (Lee 2012), metal contamination and underestimated jack-knife error bars (Rollinde et al. 2013). A recent measurement based on the cutoff in Doppler parameters of Ly α forest lines by Rudie et al. (2012) favors $\gamma \simeq 1.5$ at $z = 2.4$. We also note that a simple power-law parametrization for the temperature-density relation is unlikely to be sufficient during or immediately following reionization, as significant scatter and a departure from a single power law are expected (e.g., Bolton et al. 2004; Trac et al. 2008; Furlanetto & Oh 2009; McQuinn et al. 2009; Meiksin & Tittley 2012; Compostella et al. 2013). Nevertheless, the scaling relations in Appendix A can be used to extend our results to flatter temperature-density relations.

4.2 Photoionization rate results

Our results for the H I photoionization rate are shown in Figure 1, with the error budget is summarized in Tables 1 and 2. We find $\Gamma(z)$ to be nearly flat (to within ~ 0.1 dex) over $2 < z < 5$. There is mild evidence for evolution with redshift, but it is not highly significant given the correlated statistical errors in $\Gamma(z)$ (Table 2). Systematic errors arising from the uncertainty in γ dominate the error budget for all but the highest-redshift bin. Errors arising from the unknown degree of Jeans smoothing, in contrast, are relatively small at all redshifts (see Table 1).

We compare our results to previous measurements of Γ based on the effective Ly α optical depth from Bolton et al. (2005), Bolton & Haehnelt (2007), and Faucher-Giguère et al. (2008a) in Figure 2. To facilitate a direct comparison, in each case we plot our nominal value of Γ for the fiducial value of γ adopted in those works. The literature results have also been adjusted for cosmology.

Our results are consistent with those of Bolton et al. (2005) over $3 < z < 4$. This is not surprising since the $\tau_{\text{eff}}^{\alpha}$ and temperature values adopted in that work were similar to the ones used here, though with larger errors. A similar technique using artificial spectra was also used to determine

Table 1. Results and error budget for $\log \Gamma$. Units for Γ are 10^{-12} s^{-1} . The nominal values are for $\gamma = 1.4$. Statistical errors reflect the diagonal terms of the covariance matrix only.

z	2.40	2.80	3.20	3.60	4.00	4.40	4.75
Nominal value	0.015	-0.066	-0.103	-0.097	-0.072	-0.019	-0.029
$\tau_{\text{eff}}^{\alpha}$ errors only	± 0.040	± 0.026	± 0.018	± 0.013	± 0.012	± 0.015	± 0.026
$T(\bar{\Delta})$ errors only	± 0.016	± 0.017	± 0.021	± 0.028	± 0.035	± 0.043	± 0.056
Cosmology errors only	± 0.019	± 0.019	± 0.020	± 0.021	± 0.022	± 0.023	± 0.024
Total statistical error	± 0.047	± 0.037	± 0.036	± 0.038	± 0.043	± 0.052	± 0.070
$\gamma = 1.6$	+0.084	+0.086	+0.083	+0.077	+0.071	+0.066	+0.064
$\gamma = 1.2$	-0.084	-0.086	-0.083	-0.077	-0.071	-0.066	-0.064
Jeans smoothing	+0.001 -0.016	+0.006 -0.008	+0.012 -0.003	+0.016 -0.003	+0.021 -0.004	+0.023 -0.005	+0.023 -0.014
Total systematic error	+0.085 -0.100	+0.092 -0.095	+0.095 -0.085	+0.094 -0.080	+0.092 -0.075	+0.089 -0.071	+0.086 -0.077
Total error	+0.132 -0.146	+0.129 -0.131	+0.130 -0.121	+0.131 -0.118	+0.135 -0.117	+0.140 -0.122	+0.156 -0.147

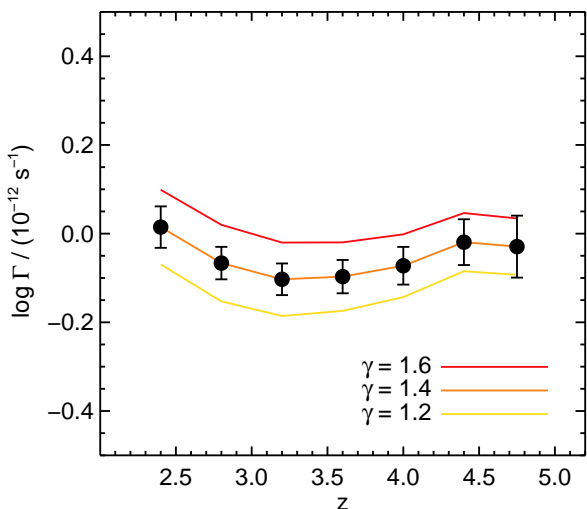


Figure 1. The hydrogen ionization rate as a function of redshift. Solid points with 1σ statistical error bars give the best-fitting Γ for our fiducial parameter for the temperature-density relation ($\gamma = 1.4$). Solid lines give Γ for $\gamma = [1.6, 1.4, 1.2]$ (top to bottom). Additional, smaller systematic uncertainties related to the density field are summarized in Table 1.

Table 2. Covariance matrix for the statistical errors in $\log \Gamma$. Values have been multiplied by 100.

z	2.40	2.80	3.20	3.60	4.00	4.40	4.75
2.40	0.218	0.142	0.112	0.091	0.079	0.073	0.069
2.80		0.134	0.097	0.074	0.068	0.064	0.057
3.20			0.127	0.085	0.063	0.064	0.064
3.60				0.141	0.086	0.058	0.062
4.00					0.181	0.107	0.063
4.40						0.267	0.164
4.75							0.488

the ionization rate. A possible break between our value of Γ at $z = 4.75$ and that of Bolton & Haehnelt (2007) at $z = 5$ may be present, but we defer discussion of the evolution of Γ at $z > 5$ to Section 7.

We are systematically higher by roughly a factor of two

than the results of Faucher-Giguère et al. (2008a). Much of this difference can be attributed to differences in the gas temperatures. Faucher-Giguère et al. (2008a) adopt T_0 values from Zaldarriaga et al. (2001), which, for their adopted value of $\gamma = 1.6$, are roughly a factor of two larger than the temperatures measured by Becker et al. (2011). The higher temperatures will produce values of Γ that are ~ 0.2 dex lower. Part of the remaining difference may relate to the different methods used to compute Γ . Faucher-Giguère et al. (2008a) derived their Γ values by directly integrating Ly α optical depths over a density distribution function in order to predict the mean transmitted flux. This neglects the effects of peculiar velocities and thermal broadening, which we incorporate by using mock spectra drawn from numerical simulations. Peculiar velocities tend to consolidate optical depth in redshift space due to the infall of gas towards filaments, thus requiring a lower ionization rate to achieve a given mean flux. In tests where we ignored peculiar velocities we obtained a higher Γ by ~ 3 (30) per cent at $z \simeq 2$ (4). Thermal broadening, in contrast, tends to increase the amount of absorption by lines of high optical depth. When we ignored thermal broadening, our results for Γ decreased by ~ 38 (26) per cent at $z \simeq 2$ (4). The net result of ignoring both peculiar velocities and thermal broadening was to decrease Γ by ~ 30 per cent at $z \simeq 2$ while leaving it essentially unchanged at $z \simeq 4$. This may help to explain the somewhat larger difference between our results and those of Faucher-Giguère et al. (2008a) at $z \sim 2.5$. We note that the $\tau_{\text{eff}}^{\alpha}$ values used by both works are generally consistent, and do not contribute greatly to the difference in Γ where the results overlap.

5 IONIZING EMISSIVITY

5.1 Method

In this section we turn to inferring the metagalactic ionizing emissivity from our photoionization rate measurements. The hydrogen ionization rate inferred from the Ly α forest opacity reflects the intensity of the UVB after processing by the IGM. In order to use this to infer the net rate at which ionizing photons are being emitted by all sources, radiative transfer effects must be taken into account. The ionization rate is related to the mean specific intensity, $J(\nu)$, by equation (1). For our calculations we

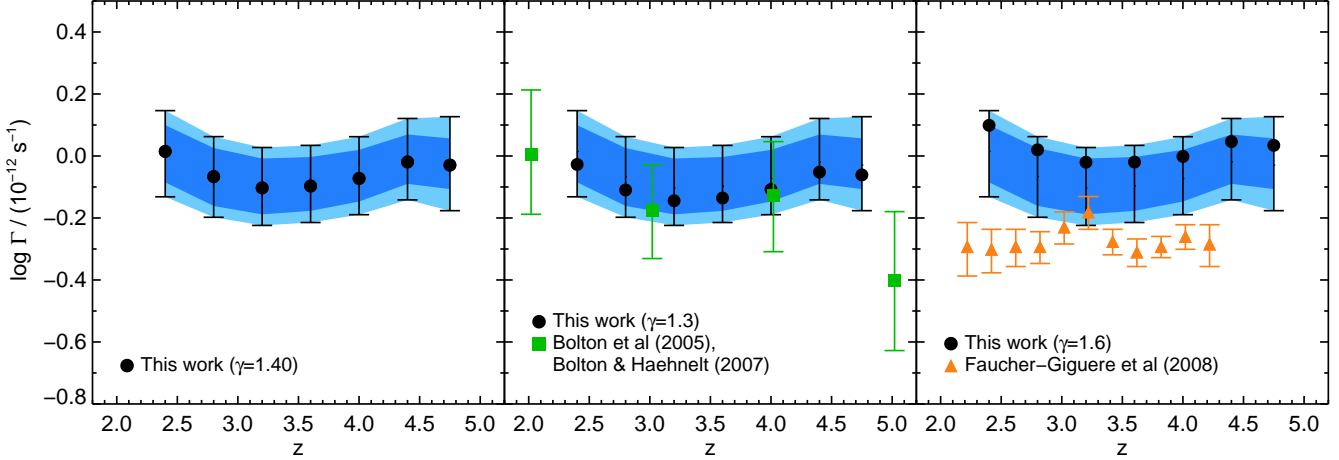


Figure 2. The hydrogen ionization rate, Γ , along with literature values over $2 < z < 5$. In each panel the inner shaded band gives the total range of systematic uncertainty, while the outer shaded band gives the total statistical error. In the left-hand panel the filled circles show the nominal values of Γ for our fiducial model with $\gamma = 1.4$. In the middle and left-hand panels, the filled circles show Γ for values of γ corresponding to those adopted in previous works (Bolton et al. 2005; Bolton & Haehnelt 2007; Faucher-Giguère et al. 2008a). Literature values have been adjusted for cosmology. Note that the error bars for Bolton et al. (2005) and Bolton & Haehnelt (2007) include uncertainties in τ_{eff} , T_0 , γ (with $1.0 \leq \gamma \leq 1.6$), and cosmological parameters, while the Faucher-Giguère et al. (2008a) errors reflect only uncertainties in τ_{eff} and T_0 . We find roughly a factor of two higher values of Γ compared to Faucher-Giguère et al. (2008a) due to the fact that we use measured temperatures that are significantly lower, and because our values are derived from artificial spectra drawn from hydrodynamical simulations rather than purely from a density PDF. See text for details. The evolution of Γ at $z \geq 5$ is discussed in Section 7.

adopt $\sigma_{\text{HI}}(\nu) \propto \nu^{-2.75}$, which is closer to the true frequency dependence (e.g., Osterbrock & Ferland 2006) than the commonly-used ν^{-3} approximation, at least over the emitted frequency range that dominates the H I ionization rate ($1 \text{ Ryd} \leq h\nu \lesssim 2 \text{ Ryd}$). This choice, however, has little impact on our results. The mean specific intensity at redshift z_0 and frequency ν_0 , in turn, can be written as an integral over the emissivity, $\epsilon(\nu, z)$, from all sources at $z \geq z_0$ as (e.g., Haardt & Madau 1996)

$$J(\nu_0, z_0) = \frac{1}{4\pi} \int_{z_0}^{\infty} dz \frac{dl}{dz} \frac{(1+z_0)^3}{(1+z)^3} \epsilon(\nu, z) e^{-\tau_{\text{eff}}(\nu_0, z_0, z)}, \quad (3)$$

where $\nu = \nu_0(1+z)/(1+z_0)$, $dl/dz = c/[(1+z)H(z)]$ is the proper line element, and $\tau_{\text{eff}}(\nu_0, z_0, z)$ is the effective optical depth for photons with frequency ν_0 at redshift z_0 that were emitted at redshift z . We note that equation (3) takes into account cosmological radiative transfer effects, including the redshifting of ionizing photons.

It is common to simplify equation (3) by assuming that the mean free path to ionizing photons is sufficiently short that the ionizing sources are essentially local. In this case, redshifting effects may be neglected and $J(\nu, z) \approx (1/4\pi)\lambda_{\text{mfp}}(\nu, z)\epsilon(\nu, z)$, where λ_{mfp} is the mean free path. As we demonstrate in Appendix C, however, this approximation can produce considerable underestimates of the ionizing emissivity, up to a factor of two at $z \sim 2$. This occurs because the local source approximation neglects the fact that at $z < 4$ a significant fraction of the ionizing photons emitted will redshift beyond the Lyman limit without being absorbed by the IGM. This loss of ionizing photons must be taken into account in order to calculate the total ionizing emissivity from the hydrogen ionization rate.

For Poisson-distributed absorbers with a column density distribution $f(N_{\text{HI}}, z) = \partial^2 \mathcal{N} / \partial N_{\text{HI}} \partial z$, $\tau_{\text{eff}}(\nu_0, z_0, z)$ can be calculated as (Paresce et al. 1980)

$$\tau_{\text{eff}}(\nu_0, z_0, z) = \int_{z_0}^z dz' \int_0^{\infty} dN_{\text{HI}} f(N_{\text{HI}}, z') (1 - e^{-\tau_\nu}), \quad (4)$$

where $\tau_\nu = N_{\text{HI}}\sigma_\nu$. It has been shown that $f(N_{\text{HI}}, z)$ has a complex shape over column densities that provide most of the optical depth to ionizing photons ($10^{15} \text{ cm}^{-2} \lesssim N_{\text{HI}} \lesssim 10^{20} \text{ cm}^{-2}$) (e.g., O’Meara et al. 2007; Prochaska et al. 2010). Ideally one would integrate equation (4) over a detailed fit to the column density distribution (e.g., Haardt & Madau 2012); however, large uncertainties exist in the amplitude of $f(N_{\text{HI}}, z)$ at column densities within the range of interest, up to an order of magnitude at $N_{\text{HI}} = 10^{17} \text{ cm}^{-2}$ (Prochaska et al. 2010; O’Meara et al. 2013). Rather than attempt to integrate over the detailed column density distribution, therefore, we follow the common convention of approximating $f(N_{\text{HI}}, z)$ as a power law of the form

$$f(N_{\text{HI}}, z) = \frac{A}{N_{\text{LL}}} \left(\frac{N_{\text{HI}}}{N_{\text{LL}}} \right)^{-\beta_N} \left(\frac{1+z}{4.5} \right)^{\beta_z} \quad (5)$$

where $N_{\text{LL}} = 10^{17.2} \text{ cm}^{-2}$ is the Lyman limit column density. Although this is a rough approximation, we have the advantage that recent works analyzing composite quasar spectra have provided direct measurements of the integrated opacity at $h\nu_0 = 1 \text{ Ryd}$, independent of the shape of $f(N_{\text{HI}}, z)$. With these measurements as an anchor point, our main requirement is to model $f(N_{\text{HI}}, z)$ with sufficient accuracy to determine the opacity at higher energies. This depends mainly on the relative contribution to $\tau_{\text{eff}}(\nu_0, z_0, z)$ from optically thin and thick systems. If the ionizing opacity

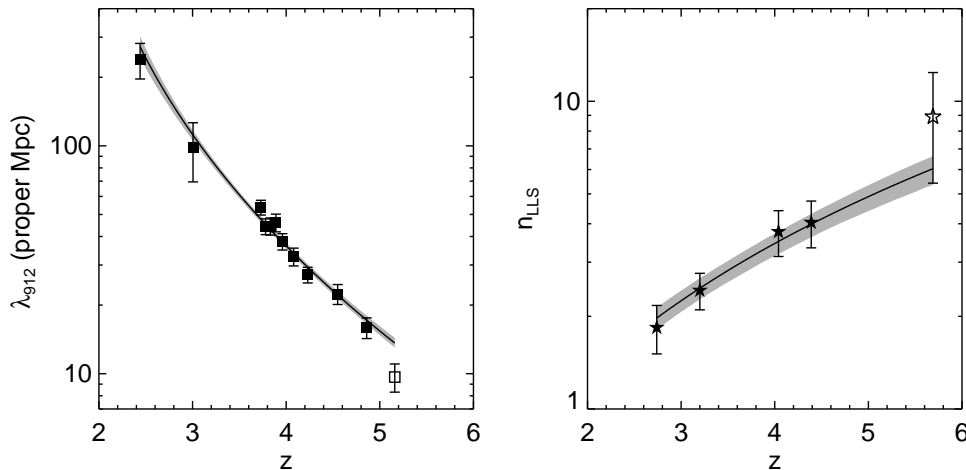


Figure 3. Parameters describing the opacity of the IGM to ionizing photons. The left panel shows the mean free path at 912 Å, with data points taken from O’Meara et al. (2013) ($z = 2.4$), Fumagalli et al. (2013) ($z = 3.0$), Prochaska et al. (2009) ($3.73 \geq z \geq 4.23$), and Worseck et al., in prep ($4.55 \geq z \geq 5.16$), with updates as compiled in Worseck et al. The right-hand panel shows the number density of Lyman limit systems, with data from Songaila & Cowie (2010). The solid lines in each panel show our fit to these quantities assuming that the H I column density distribution has the form $f(N_{\text{HI}}, z) \propto N_{\text{HI}}^{-\beta_N} (1+z)^{\beta_z}$. Shaded regions show the 1σ uncertainty in the fit. Data with empty symbols were not included in the fit, as they lie outside the redshift range covered by our analysis. For the sake of comparison, however, we plot the fits extrapolated to these redshifts.

is mainly due to optically thin systems, then the mean free path as a function of frequency will scale inversely with the ionization cross section, $\lambda_{\text{mfp}, \nu}^{\text{thin}} \propto \sigma_{\nu}^{-1} \propto \nu^{2.75}$. If instead the opacity comes from optically thick ‘bricks’, then the mean free path will be independent of frequency. A power law approximation to the column density distribution provides a convenient means to quantify this balance, at least to first order, as well as to simplify the calculation of $\tau_{\text{eff}}(\nu_0, z_0, z)$.

We determine the parameters for $f(N_{\text{HI}}, z)$ in equation (5) by combining direct measurements of the mean free path for 1 Ryd photons, λ_{912} , with measurements of the number density of Lyman limit systems ($N_{\text{HI}} \geq 10^{17.2} \text{ cm}^{-2}$). The λ_{912} values were determined directly from the flux profiles of composite quasar spectra by Prochaska et al. (2009), O’Meara et al. (2013), Fumagalli et al. (2013), and Worseck et al. (in prep). We note that $\lambda(z)$ is defined here as a function of the emitted redshift, in the sense that a packet of photons emitted at redshift z with frequency $\nu = \nu_0(1+z)/(1+z_0)$ travels a distance λ to redshift z_0 , by which point their frequency is ν_0 and the number of photons is diminished, on average, by a factor of e . Thus, λ_{912} refers to the mean free path for photons emitted with energy greater than 1 Ryd. Values for the number density of Lyman limit systems, n_{LLS} , were taken from Songaila & Cowie (2010), who also included measurements compiled by Péroux et al. (2003). We note that other works have used n_{LLS} to infer λ_{912} , which requires assuming a slope for $f(N_{\text{HI}})$ near the Lyman limit (e.g., Madau et al. 1999; Kuhlen & Faucher-Giguère 2012). Here, however, we are combining independent measurements of λ_{912} and n_{LLS} to constrain β_N . We emphasize again that this is really an effective slope for $f(N_{\text{HI}}, z)$ intended only to facilitate the calculation of the ionizing opacity as a function of frequency and redshift. It will therefore not reflect the full details of the H I column density distribution.

The parameters A , β_N , and β_z are determined by simultaneously fitting the λ_{912} and n_{LLS} values as a function of redshift. The number density of Lyman limit systems is obtained by directly integrating $f(N_{\text{HI}}, z)$ over column density to obtain $n_{\text{LLS}}(z)$. We use equation (4) to determine z_0 at which $\tau_{\text{eff}}(\nu_{912}, z_0, z) = 1$, and then convert this into a mean free path at the Lyman limit by computing the proper distance between z and z_0 . We integrate equation (4) over a finite range in H I column density with nominal limits of $[N_{\text{HI}}^{\text{min}}, N_{\text{HI}}^{\text{max}}] = [10^{15}, 10^{21}] \text{ cm}^{-2}$. These limits are meant to span the range in N_{HI} that dominates the optical depth to ionizing photons (e.g., Haardt & Madau 2012, and references therein), such that our power-law approximation for $f(N_{\text{HI}}, z)$ most closely matches the true shape of the column density distribution over this range. We found our results for $f(N_{\text{HI}}, z)$ and the emissivity to be insensitive to the lower limit of integration for $N_{\text{HI}}^{\text{min}} \leq 10^{16} \text{ cm}^{-2}$. Increasing the upper limit will tend to flatten $f(N_{\text{HI}})$ and decrease A . This ultimately has only a minor impact on the calculated emissivity, however, as quantified below.

Our best-fitting parameters for $f(N_{\text{HI}}, z)$ are $[A, \beta_N, \beta_z] = [0.93 \pm 0.08, 1.33 \pm 0.05, 1.92 \pm 0.15]$, where the errors in A and β_N are highly correlated. The accompanying fits to $\lambda_{912}(z)$ and $n_{\text{LLS}}(z)$ are plotted in Figure 3. This fit also produces a number density of LLSs with $\tau > 2$ that is consistent at the $<1.5\sigma$ level with measurements over $2 \lesssim z \lesssim 4$ (Prochaska et al. 2010; O’Meara et al. 2013; Fumagalli et al. 2013). Uncertainties in the parameters were determined by perturbing the data points according to their errors and re-calculating the fit. The corresponding errors in our fits to $\lambda_{912}(z)$ and $n_{\text{LLS}}(z)$ are shown as shaded regions in Figure 3.¹

¹ We note that despite the fact that we are consistent with the $n_{\text{LLS}}(z)$ values of Songaila & Cowie (2010), by design, and our best-fit value of β_N is similar to the one used by those authors,

We note that our results are not highly sensitive to exact value of β_N , provided that we fit the λ_{912} values. For example, if we fix β_N to be 1.5 (e.g., Madau et al. 1999, and references therein), and refit for A and β_z , our estimates of the emissivity would decrease by less than 12 per cent versus the nominal values. Doing so would underestimate the number density of LLSs. To be conservative, however, we adopt an additional systematic uncertainty in the emissivity related to fitting $f(N_{\text{HI}}, z)$ of ± 0.05 dex.

In order to address whether approximating $f(N_{\text{HI}}, z)$ as a single power law may bias our emissivity estimates, we performed the following test. We first generated an artificial data set by calculating the predicted values for $\lambda_{912}(z)$ and $n_{\text{LLS}}(z)$ over $2.4 < z < 5$ from the piece-wise fit to $f(N_{\text{HI}}, z)$ adopted by Haardt & Madau (2012). We then fit a single power law $f(N_{\text{HI}}, z)$ to these values following the procedure described above, finding $[A, \beta_N, \beta_z] = [1.05, 1.52, 1.91]$. Next we calculated the emissivity using the Haardt & Madau (2012) piece-wise fit directly and using the single power law approximation. For a fixed $\Gamma(z)$, the single power law produced emissivity results that were 5-19 per cent lower than those obtained using the piece-wise $f(N_{\text{HI}}, z)$. The bias was found to increase with increasing redshift and for harder ionizing spectra (see below). These results suggest that for the narrow purpose of estimating the emissivity near 1 Ryd, a single power law model for $f(N_{\text{HI}}, z)$ is a reasonable approximation provided that it reproduces the correct λ_{912} and n_{LLS} values. The precise level of bias will depend on the details of the true H I column density distribution. Taking these results as a guide, however, we apply a positive 10 percent correction to our raw emissivity values, and increase the systematic uncertainty related to fitting $f(N_{\text{HI}}, z)$ by a further ± 0.05 dex.

We follow the common convention of modeling the spectral shape of the specific emissivity as a power law of the form

$$\epsilon(\nu, z) = \epsilon_{912}(z) \left(\frac{\nu}{\nu_{912}} \right)^{-\alpha}, \quad (6)$$

where ϵ_{912} is the specific emissivity at the Lyman limit and α is the spectral index blueward of the Lyman limit. The integrated emissivity of ionizing photons, \dot{N}_{ion} , is then given by

$$\dot{N}_{\text{ion}}(z) = \int_{\nu_{912}}^{\infty} d\nu \frac{\epsilon(\nu, z)}{h\nu} = \frac{\epsilon_{912}}{h\alpha}. \quad (7)$$

The most appropriate value for α is a subject of debate. For AGN, a value of $\alpha = 1.6$ (Telfer et al. 2002) is commonly used, whereas for galaxies the adopted values of α range between 1 and 3 (e.g., Bolton & Haehnelt 2007; Ouchi et al. 2009; Kuhlen & Faucher-Giguère 2012). For realistic galaxy

the values of λ_{912} adopted here are considerably larger than those derived by them and adopted by Kuhlen & Faucher-Giguère (2012) at $z \leq 3.4$. For example, the mean free path we determine from our $f(N_{\text{HI}}, z)$ fit at $z = 2.6$ is ~ 50 per cent larger than the Songaila & Cowie (2010) value. This is primarily because the Songaila & Cowie (2010) values are calculated using an expression that assumes $z_0 \simeq z$ (their equation (7); see also Madau et al. (1999), Faucher-Giguère et al. (2008a) equation (22)). This underestimated the true mean free path as defined above, particularly at $z < 4$.

spectra, however, a single power law is probably an oversimplification, even between the H I and He II ionizing edges. For example, a STARBURST99 model (Leitherer et al. 1999) with $t_{\text{age}} = 500 \text{ Myr}^2$, continuous star formation, Salpeter IMF, and metallicity $Z = (1/5)Z_{\odot}$ has a slope of $\alpha \simeq 1.3$ between 1 and 1.8 Ryd. This energy range is responsible for most of the H I photoionization events due to the steep frequency dependence of the ionizing cross section, and so this value of α is appropriate for calculating ϵ_{912} . At higher energies, however, the spectrum softens and essentially goes to zero at $E > 4$ Ryd. Integrating the model spectrum over all frequencies $\nu \geq \nu_{912}$ gives the same total number of photons as integrating over a pure power-law spectrum with $\alpha = 1.8$.³ For a STARBURST99 model with $Z = (1/20)Z_{\odot}$, the slope near 1 Ryd is ~ 1.1 , while the “effective” slope integrating over all frequencies is ~ 1.7 . For $Z = Z_{\odot}$ these values become roughly 1.5 and 2.0, respectively. Recent models using the BPASS spectral library (Eldridge & Stanway 2012) and including massive binaries give similar results at low metallicities, though the ionizing spectra are softer at solar metallicity.⁴ These examples illustrate that care must be taken when converting Γ , which is dominated by photons close to 1 Ryd, to a specific ionizing emissivity near the Lyman limit and/or a total ionizing emissivity. For simplicity, however, we will mainly treat the emitted ionizing spectrum as a single power law at $h\nu \geq 1$ Ryd. We adopt a nominal value of $\alpha = 2.0$, but also calculate ϵ_{912} and \dot{N}_{ion} for $\alpha = 1.0$ and 3.0. In addition, we perform calculations for the STARBURST99 model galaxy spectrum with $Z = (1/5)Z_{\odot}$ mentioned above.

We combine equations (1)-(7) in order to calculate ϵ_{912} and \dot{N}_{ion} from our Γ values and the ionizing opacity measurements described above. We use an analytic solution for $\tau_{\text{eff}}(\nu_{912}, z_0, z)$, which is possible for a power-law $f(N_{\text{HI}}, z)$.⁵ The remainder of our calculations are performed numerically. Since we are not using the local-source approximation, $\Gamma(z_0)$ will depend on $\epsilon_{912}(z)$ at $z \geq z_0$, and so $\epsilon_{912}(z)$ must be modeled as a continuous function in redshift. We therefore parametrize $\epsilon_{912}(z)$ at four discrete redshifts between $z = 2.4$ and 4.75, and assume that it evolves linearly between these points.

Finally, we apply an approximate correction to the emissivity to account for recombination radiation. For a given emissivity from galaxies and AGN, recombination radiation from the IGM will tend to enhance the photoionization rate (Haardt & Madau 1996, 2012; Fardal et al. 1998; Faucher-Giguère et al. 2009). We estimate the fractional increase in Γ when including this effect using the analytic ex-

² The figures given here do not depend sensitively on age, since the spectral shape blueward of 912 Å is dominated by short-lived, massive stars.

³ This STARBURST99 was previously used to motivate a model in which $\alpha = 3.0$ (e.g., Bolton & Haehnelt 2007; Ouchi et al. 2009; Nestor et al. 2013). This value reflects the ratio of luminosities at the H I and He II ionizing edges; however, between these limits the model contains considerably more flux than would an $L_{\nu} \propto \nu^{-3}$ power law with the same luminosity just below 912 Å.

⁴ We note, however, that the spectral break between 1500 Å and 912 Å, L_{1500}/L_{912} , is significantly smaller in the BPASS models for all metallicities.

⁵ See Faucher-Giguère et al. (2008a) for the case in which $[N_{\text{HI}}^{\text{min}}, N_{\text{HI}}^{\text{max}}] = [0, \infty]$.

Table 3. Results and error budget for $\log \epsilon_{912}$ and $\log \dot{N}_{\text{ion}}$. Units for ϵ_{912} are $10^{23} \text{ erg s}^{-1} \text{ Hz}^{-1} \text{ Mpc}^{-3}$. Units for \dot{N}_{ion} are $10^{51} \text{ photons s}^{-1} \text{ Mpc}^{-3}$. The nominal values are for $\gamma = 1.4$, $\alpha = 2.0$. Statistical errors reflect the diagonal terms of the covariance matrix only. Systematic errors in $f(N_{\text{HI}}, z)$ include errors arising from changes to $[N_{\text{HI}}^{\text{min}}, N_{\text{HI}}^{\text{max}}]$, possible systematic changes to β_N , and the approximation of $f(N_{\text{HI}}, z)$ as a single power law (see text).

z	$\log \epsilon_{912}$				$\log \dot{N}$			
	2.40	3.20	4.00	4.75	2.40	3.20	4.00	4.75
Nominal value	2.076	1.911	1.983	2.108	-0.046	-0.211	-0.139	-0.014
τ_{eff} errors only	± 0.048	± 0.021	± 0.015	± 0.018	± 0.048	± 0.021	± 0.015	± 0.018
$T(\Delta)$ errors only	± 0.028	± 0.032	± 0.040	± 0.040	± 0.028	± 0.032	± 0.040	± 0.040
$f(N_{\text{HI}}, z)$ stat. errors only	± 0.011	± 0.012	± 0.014	± 0.019	± 0.011	± 0.012	± 0.014	± 0.019
Cosmology errors only	± 0.017	± 0.017	± 0.019	± 0.021	± 0.017	± 0.017	± 0.019	± 0.021
Total statistical error	± 0.059	± 0.044	± 0.048	± 0.053	± 0.059	± 0.044	± 0.048	± 0.053
$\gamma = 1.6$	+0.084	+0.089	+0.074	+0.065	+0.084	+0.089	+0.074	+0.065
$\gamma = 1.2$	-0.084	-0.089	-0.075	-0.065	-0.084	-0.089	-0.075	-0.065
$\alpha = 3.0$	+0.125	+0.123	+0.119	+0.113	-0.052	-0.053	-0.057	-0.063
$\alpha = 1.0$	-0.153	-0.155	-0.151	-0.145	+0.148	+0.146	+0.150	+0.156
Jeans smoothing	+0.000 -0.022	+0.010 -0.006	+0.022 -0.003	+0.022 -0.010	+0.000 -0.022	+0.010 -0.006	+0.022 -0.003	+0.022 -0.010
$f(N_{\text{HI}}, z)$ systematics	+0.103 -0.106	+0.106 -0.111	+0.107 -0.113	+0.108 -0.114	+0.103 -0.106	+0.106 -0.111	+0.107 -0.113	+0.108 -0.114
Recombination rad. systematics	± 0.050	± 0.050	± 0.050	± 0.050	± 0.050	± 0.050	± 0.050	± 0.050
Total systematic error	+0.362 -0.415	+0.378 -0.411	+0.372 -0.392	+0.358 -0.383	+0.385 -0.313	+0.401 -0.308	+0.403 -0.298	+0.401 -0.301
Total error	+0.421 -0.474	+0.422 -0.455	+0.420 -0.440	+0.412 -0.437	+0.444 -0.372	+0.445 -0.352	+0.451 -0.346	+0.454 -0.355

Table 4. Covariance matrix for the statistical errors in $\log \epsilon_{912}$ and $\log \dot{N}_{\text{ion}}$.

z	2.40	3.20	4.00	4.75
2.40	3.46	0.74	1.18	0.49
3.20		1.95	0.03	0.69
4.00			2.28	0.19
4.75				2.84

pressions in Faucher-Giguère et al. (2009) (their Appendix C). For the $f(N_{\text{HI}}, z)$ parameters used here, and assuming a gas temperature of 10,000 K (20,000 K), we find $\Gamma^{\text{with rec}}/\Gamma^{\text{no rec}} \simeq 1.05 - 1.12$ ($1.08 - 1.15$) over $2.4 \leq z \leq 4.75$, where the effect increases with redshift. This is similar to, though slightly lower than, the amplitude found by Faucher-Giguère et al. (2009) for their fiducial set of parameters. As explored by those authors, the precise impact of recombination radiation will depend on the details of the H I column density distribution and the temperature structure of the IGM, which are only approximately modeled here. As a first-order correction, therefore, we simply decrease our emissivity results by 10 per cent (offsetting the above correction related to $f(N_{\text{HI}}, z)$), but include an additional ± 0.05 dex systematic uncertainty.

5.2 Emissivity results

Our results for ϵ_{912} and \dot{N}_{ion} are presented in Figures 4 and 5, respectively, with the error budget summarized in Tables 3 and 4. The statistical errors in the emissivity reflect the statistical errors in Γ (from τ_{eff}^α and $T(\bar{\Delta})$), λ_{912} , and n_{LLS} , as well in the cosmology. Systematic errors from the slope of the temperature-density relation and spectral slope are shown separately. We also list smaller systematic errors related to

Jeans smoothing, $f(N_{\text{HI}}, z)$ fitting, and recombination radiation (see above). Uncertainties in γ produce systematic uncertainties in ϵ_{912} and \dot{N}_{ion} that are comparable to the 1σ statistical errors. Increasing α from 2.0 to 3.0 increases ϵ_{912} by 0.11-0.13 dex, while decreasing α from 2.0 to 1.0 decreases ϵ_{912} by 0.13-0.16 dex. Conversely, increasing α from 2.0 to 3.0 decrease \dot{N}_{ion} by 0.05-0.07 dex, while decreasing α from 2.0 to 1.0 increases \dot{N}_{ion} by 0.15-0.17 dex. This occurs because a harder emitted spectrum means that a larger proportion of ionizing photons are emitted at frequencies where the ionization cross-section is small, thus making a smaller contribution to Γ .

We include estimates for ϵ_{912} and \dot{N}_{ion} for a STAR-BURST99 model with continuous star formation and $Z = (1/5)Z_\odot$ in the right-hand panels of Figures 4 and 5. Note that, in this case, adopting a more complex ionizing spectrum decreases both ϵ_{912} and \dot{N}_{ion} . This happens because the spectrum has a relatively shallow slope near the Lyman limit, allowing a lower ϵ_{912} , but then steepens at higher energies, decreasing the total \dot{N}_{ion} .

Although ϵ_{912} and \dot{N}_{ion} may exhibit some evolution with redshift within the statistical errors alone, the degree to which these quantities truly change with redshift largely depends on how the temperature-density relation slope, γ , and spectral shape of the emissivity, α , evolve. Here we note, however, that the total emissivity at $z = 4.75$ is quite substantial, with $\dot{N}_{\text{ion}} \sim 5$ ionizing photons per atom per gigayear for our fiducial values of γ and α , or for the example galaxy model spectrum. \dot{N}_{ion} may potentially be as high as ~ 14 photons/atom/Gyr at $z = 4.75$, but this is only for $\alpha = 1.0$, with no softening or break towards higher energies, and a maximally steep temperature-density relation ($\gamma = 1.6$).

We compare our results to previous estimates of \dot{N}_{ion} in Figure 6. To facilitate a direct comparison, we present

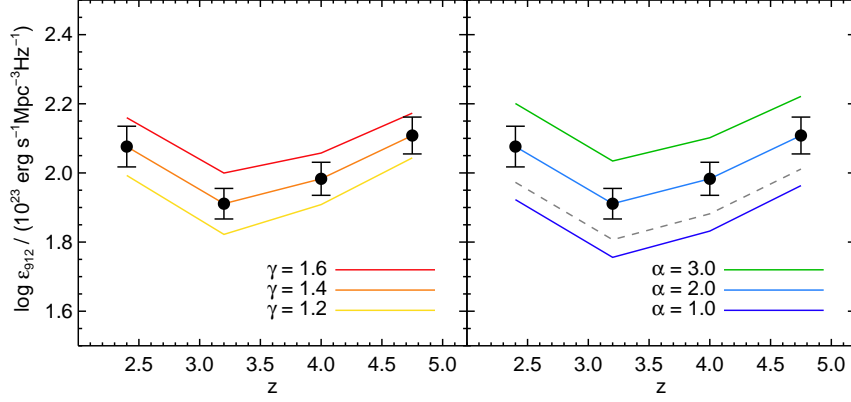


Figure 4. The specific emissivity near the Lyman limit as a function of redshift. Filled circles with 1σ statistical error bars show ϵ_{912} for our fiducial temperature-density parameter ($\gamma = 1.4$) and spectral index of the ionizing sources ($\alpha = 2.0$). In the left-hand panel, solid lines give ϵ_{912} for $\gamma = [1.6, 1.4, 1.2]$ (top to bottom). In the right-hand panel, solid lines give ϵ_{912} for $\alpha = [1.0, 2.0, 3.0]$ (bottom to top). The dashed line gives approximate values for a STARBURST99 model with continuous star formation and $Z = (1/5)Z_{\odot}$ (see text). Additional, smaller systematic uncertainties are summarized in Table 3.

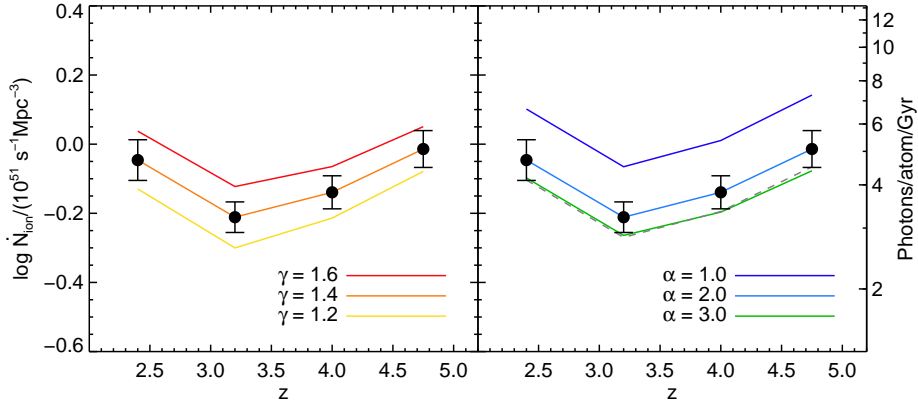


Figure 5. The integrated emissivity of ionizing photons as a function of redshift. Filled circles with 1σ statistical error bars show \dot{N}_{ion} for our fiducial temperature-density parameter ($\gamma = 1.4$) and spectral index of the ionizing sources ($\alpha = 2.0$). In the left-hand panel, solid lines give \dot{N}_{ion} for $\gamma = [1.6, 1.4, 1.2]$ (top to bottom). In the right-hand panel, solid lines give \dot{N}_{ion} for $\alpha = [1.0, 2.0, 3.0]$ (bottom to top). The dashed line gives approximate values for a STARBURST99 model with continuous star formation and $Z = (1/5)Z_{\odot}$ (see text). Additional, smaller systematic uncertainties are summarized in Table 3.

our results for the same set of γ and α values used in the previous works⁶. Minor corrections have been applied to the literature results to reflect our adopted $\nu^{-2.75}$ frequency dependence for the ionizing cross-section. Corrections for cosmology have also been applied, although we have not attempted to propagate these through to the Bolton & Haehnelt (2007) estimates of the mean free path, which are based on modeling self-shielded gas in a hydrodynamical simulation, and, as discussed by these authors, are uncertain to within a factor of two. We note that the errors on the Bolton & Haehnelt (2007) values of \dot{N}_{ion} are probably too small due to the degeneracy between Γ and λ_{912} in their model; therefore, only their nominal values for \dot{N}_{ion} are shown in Figure 6. Finally, we have also made small adjustments to the Kuhlen & Faucher-Giguère (2012) values such

that \dot{N}_{ion} is integrated over all frequencies $\nu \geq \nu_{912}$, rather than only between the H I and He II ionizing edges.

Our results are nominally ~ 40 per cent higher than those of Bolton & Haehnelt (2007) at $z \simeq 3$. This reflects the fact that we obtain similar values for Γ and λ_{912} at this redshift, while a potential increase in the Bolton & Haehnelt (2007) value of \dot{N}_{ion} due to the fact that they assume no modification of the ionizing spectrum due to absorption by the IGM is more than offset by a decrease due to the fact that they use a local-source approximation to calculate \dot{N}_{ion} (see Appendix C). At $z = 4$ their value falls a factor of ~ 1.8 below our result, mainly due to the fact that they calculate a mean free path which is ~ 60 per cent larger at $z = 4$ than the one used here. The factor of ~ 2.5 difference at $z \sim 5$ is due to their use of both a larger λ_{912} and a lower Γ .

Our results generally overlap with those of Kuhlen & Faucher-Giguère (2012) within the broad errors adopted by both works; however, our nominal values for \dot{N}_{ion} are a factor of two to six higher for the same values

⁶ Values in Kuhlen & Faucher-Giguère (2012) Table 2 are for $\alpha = 3.0$, although a fiducial values of 1.0 is stated in the text.

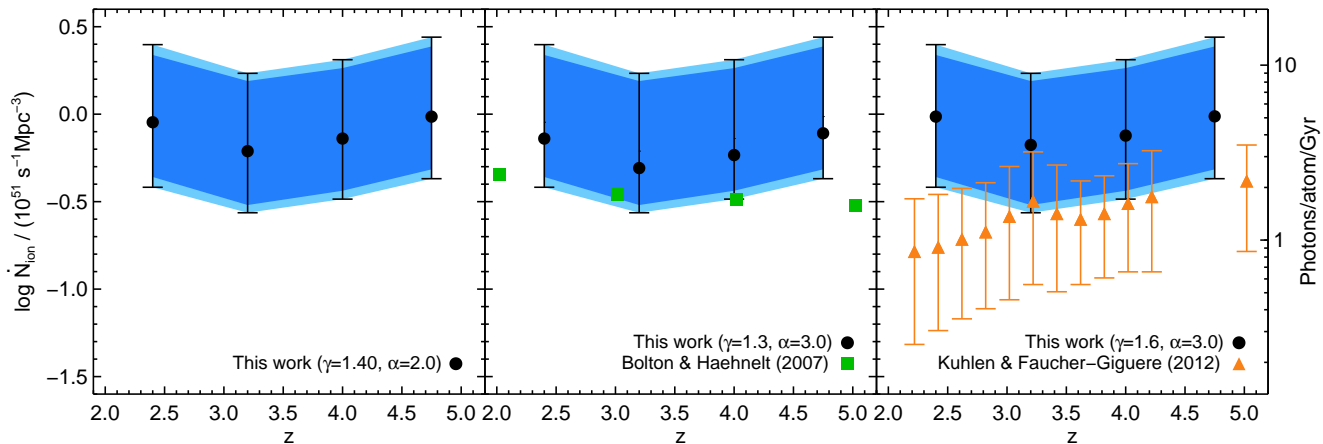


Figure 6. Integrated emissivity of ionizing photons, \dot{N}_{ion} , along with literature values over $2 < z < 5$. In each panel the inner shaded band gives the total range of systematic uncertainty, while the outer shaded band gives the total statistical error. In the left-hand panel the filled circles show the nominal values of \dot{N}_{ion} for our fiducial model with $\gamma = 1.4$ and $\alpha = 2.0$. In the middle and left-hand panels, the filled circles show \dot{N}_{ion} for values of γ and α corresponding to those adopted in previous works (Bolton & Haehnelt 2007; Kuhlen & Faucher-Giguère 2012). The Kuhlen & Faucher-Giguère (2012) value at $z = 5$ was calculated using Γ from Bolton & Haehnelt (2007). Literature values have been adjusted for cosmology and to reflect a $\sigma_{\nu} \propto \nu^{-2.75}$ scaling of the H I ionization cross section. The Kuhlen & Faucher-Giguère (2012) values have also been adjusted to give results integrated over all frequencies $\nu > \nu_{912}$. Differences between our results and those of previous works are related mainly to the combined differences in Γ and the ionizing opacity, as well as to the fact that we include radiative transfer effects when computing \dot{N}_{ion} . See text for details.

of γ and α . The factor of six discrepancy at $z = 2.4$ is partially explained by the fact that the Γ value they adopt from Faucher-Giguère et al. (2008a) is a factor of ~ 2.5 lower than our own at this redshift. As discussed above, this is due to the differences in the gas temperatures and the fact that our results are based on artificial spectra drawn from hydrodynamical simulations. An additional factor of two comes from the fact that they use a local source approximation to compute the mean free path and \dot{N}_{ion} (see Appendix C). The remaining factor of ~ 1.2 reflects small differences in the adopted shape of $f(N_{\text{HI}}, z)$ used to compute the mean free path (see Songaila & Cowie 2010), as well as the fact that our Γ values formally decrease from $z = 2.4$ to 3.2, which amplifies the radiative transfer effect somewhat above the case discussed in Appendix C.

6 THE SOURCES OF IONIZING PHOTONS

Our estimates for the ionizing emissivity are based on the physical conditions of the IGM and include the ionizing output from all sources. We now turn towards disentangling the contributions from AGN and galaxies, and using the results to infer possible trends in the ionizing efficiency of galaxies in the post-reionization era.

For the ionizing emissivity of AGN we adopt estimates made by Cowie et al. (2009). This work combined direct measurements of the ionizing and near-UV luminosities of AGN at $z \sim 1$ with the evolution of the near-UV luminosity density in an X-ray selected sample of broad-line AGN over $0 < z < 5$. We compare their results for the specific emissivity from AGN at 912 \AA to our results for the total specific emissivity from all sources in Figure 7. The Cowie et al. (2009) estimate of the AGN contribution falls well below the total emissivity, and becomes an increasingly small frac-

tion towards higher redshifts. We calculate the contribution from galaxies, $\epsilon_{912}^{\text{G}}$, by subtracting the AGN estimate from our total values, linearly interpolating the Cowie et al. (2009) AGN measurements onto our redshift bins and using a Monte Carlo approach to propagate the errors. Our estimates of the galaxy emissivity are shown in Figure 7. The galaxy and AGN contributions are potentially comparable, at least to within the errors, at $z \simeq 2.4$. At higher redshifts, however, the galaxies increasingly dominate the ionizing emissivity, producing essentially all of the ionizing photons just below the Lyman limit at $z \geq 4$. These results are consistent with a picture in which galaxies provide most of the ionizing photons during hydrogen reionization ($z > 6$), but also indicate that the contribution from galaxies remains dominant down to much lower redshifts.

The contribution of AGN to the UV background is a subject of ongoing debate (for a recent discussion see Fontanot et al. 2012). Haardt & Madau (2012), for example, adopt an AGN ionizing emissivity based on bolometric luminosity functions compiled by Hopkins et al. (2007) that is roughly a factor of two higher than the Cowie et al. (2009) estimates. We show the Haardt & Madau (2012) model as a dotted line in Figure 7. For these values, AGN are sufficient to produce essentially all of the ionizing emissivity at $z = 2.4$ and 3.2, though they would still be strongly subdominant at $z \geq 4$. For this paper we adopt the Cowie et al. (2009) estimate of the AGN emissivity since it is based on direct measurements of the ionizing flux. We will argue below that the flat or increasing galaxy emissivity towards higher redshifts indicates that the efficiency with which galaxies emit ionizing photons, relative to their non-ionizing UV output, must increase strongly from $z \sim 3$ to 5. If we instead adopt the Haardt & Madau (2012) AGN emissivity, then the evolution in the galaxy emissivity would be even more pronounced, strengthening this conclusion.

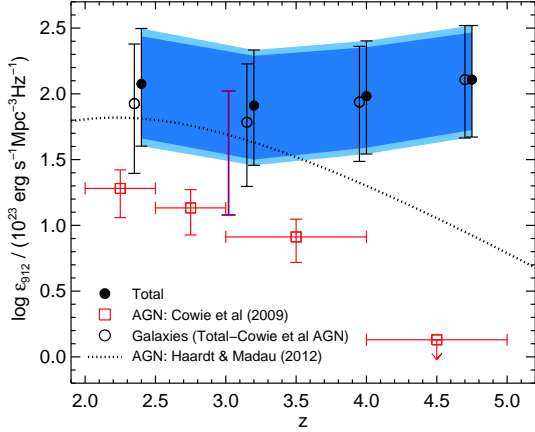


Figure 7. The specific emissivity at 912 Å. Filled circles give our results for our fiducial parameters ($\gamma = 1.4$, $\alpha = 2.0$). The inner shaded band gives the total range of systematic uncertainty, while the outer shaded band gives the total statistical error. Estimates of the AGN emissivity from Cowie et al. (2009) are shown as open squares, while the dotted line is the model AGN emissivity adopted by Haardt & Madau (2012). The open circles give our results after subtracting the Cowie et al. (2009) estimate of the AGN contribution. The error bar at $z = 3.0$ is an estimate of the contribution of galaxies to ϵ_{912} based on direct measurements of escaping ionizing radiation from LBGs and LAEs (see text).

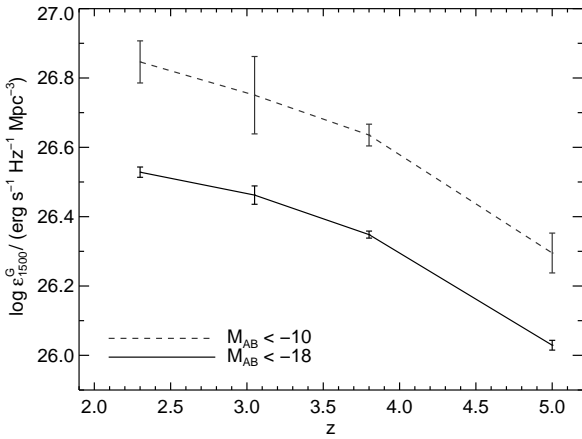


Figure 8. The non-ionizing specific UV emissivity at 1500 Å from dropout-selected galaxies determined from the luminosity functions of Reddy & Steidel (2009) ($z = 2.3$ and 3.05) and Bouwens et al. (2007) ($z = 3.8$ and 5.0). The solid and dashed lines show the results when integrating down to $M_{\text{AB}} = -18$ and -10 , respectively.

With an estimate for the ionizing emissivity of galaxies over $2 < z < 5$ in hand, we can now attempt to gain some insight into the evolution of star-forming galaxies at high redshifts by comparing $\epsilon_{912}^{\text{G}}$ to the integrated galaxy emissivity in the non-ionizing UV continuum, which essentially traces the unobscured star formation rate density. For this we use the ~ 1500 Å rest-frame luminosity functions of dropout selected galaxies from Reddy & Steidel (2009) at $z = 2.3$ and $z = 3.05$, and from Bouwens et al. (2007) at $z = 3.80$ and $z = 5.0$, each of which extends signifi-

cantly over the faint end. We calculate the non-ionizing UV emissivity⁷, $\epsilon_{1500}^{\text{G}}$, integrated over $M_{\text{AB}} \leq -18$ (roughly the observational limit) and $M_{\text{AB}} \leq -10$ using the published luminosity function parameters. Error estimates for $\epsilon_{1500}^{\text{G}}$ are determined using a Monte Carlo approach whereby we perturb the binned luminosity functions by their errors, fit a new luminosity function to the results, and integrate over the new fit. The results, which are similar to those obtained by Robertson et al. (2013) at $z = 5$, are plotted in Figure 8. The increase when integrating down to $M_{\text{AB}} = -10$ is consistently a factor of ~ 2 over this redshift range, due to the fact the faint-end slope remains roughly constant near -1.7 .

We compute the ratio of ionizing to non-ionizing galaxy emissivity, $\epsilon_{912}^{\text{G}}/\epsilon_{1500}^{\text{G}}$, by interpolating the $\epsilon_{1500}^{\text{G}}$ values from Figure 8 onto the redshifts where we measure $\epsilon_{912}^{\text{G}}$, and again using a Monte Carlo approach to propagate the errors. The results are plotted in Figure 9 for the case where $\epsilon_{1500}^{\text{G}}$ is integrated down to $M_{\text{AB}} = -18$. For our fiducial parameters ($\gamma = 1.4$, $\alpha = 2.0$), $\epsilon_{912}^{\text{G}}/\epsilon_{1500}^{\text{G}}$ is flat from $z = 2.4$ to 3.2 , but then increases by a factor of ~ 4 from $z = 3.2$ to 4.75 . This change is driven roughly equally by the decline in $\epsilon_{1500}^{\text{G}}$ and the increase in $\epsilon_{912}^{\text{G}}$. Systematic uncertainties are once again considerable, particularly those related to α . The combined errors are plotted in Figure 10, where we give the emissivity ratio when integrating $\epsilon_{1500}^{\text{G}}$ down to both $M_{\text{AB}} = -18$ and -10 . The systematic uncertainties formally permit $\epsilon_{912}^{\text{G}}/\epsilon_{1500}^{\text{G}}$ to remain nearly constant over $2.4 < z < 4.75$. This requires that γ generally increases with decreasing redshift, a plausible scenario if the temperature-density relation is somewhat flat at $z \sim 5$. More significantly, however, a constant $\epsilon_{912}^{\text{G}}/\epsilon_{1500}^{\text{G}}$ requires that the spectra of the ionizing sources just below the H I ionization edge become much softer towards lower redshifts ($\alpha \simeq 1$ at $z = 4.75$ to $\alpha \simeq 3$ at $z = 3.2$). The mean galaxy spectrum may soften somewhat as stellar populations become more metal rich, but even at solar metallicity, population synthesis models predict $\alpha \lesssim 2$ just below 1 Ryd, versus $\alpha \simeq 1.0 - 1.3$ for $Z \leq (1/5)Z_{\odot}$ (Leitherer et al. 1999; Eldridge & Stanway 2012). It therefore appears likely that the ratio of ionizing to non-ionizing output from galaxies increases towards higher redshifts. As noted above, this trend would be exaggerated (by roughly a factor of two) if we adopted the AGN emissivity from Haardt & Madau (2012). Doing so would decrease $\epsilon_{912}^{\text{G}}$ from galaxies over $2.4 \leq z \leq 3.2$, while leaving it largely unchanged at $z = 4.75$. We show the nominal results for $\epsilon_{912}^{\text{G}}/\epsilon_{1500}^{\text{G}}$ under this scenario as a dotted line in Figure 10.

7 DISCUSSION

7.1 Comparison with direct measurements of galaxy ionizing emissivity

We now address whether our estimates of the ionizing emissivity are compatible with what has been directly observed at high redshifts. Nestor et al. (2013) and Mostardi et al. (2013) recently used narrow-band imaging to measure the ionizing UV luminosities of large samples of spectroscopically-confirmed $z \sim 3$ color-selected Lyman

⁷ In the literature on high-redshift galaxies the specific emissivity is sometimes referred to as the UV luminosity density, ρ_{UV} .

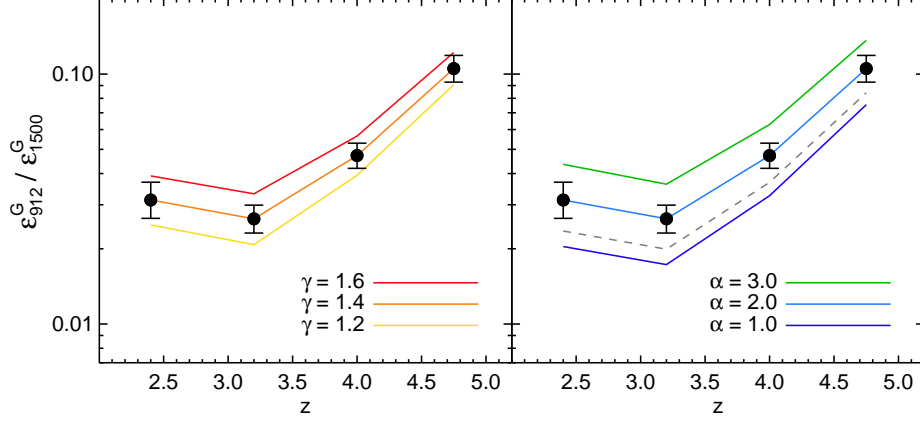


Figure 9. The ratio of ionizing to non-ionizing specific UV emissivity from galaxies. Filled circles with 1σ statistical error bars show the results for our fiducial parameters ($\gamma = 1.4$, $\alpha = 2.0$) and when integrating the luminosity density at 1500 \AA down to $M_{\text{AB}} = -18$. In the left-hand panel, solid lines reflect the change in ϵ_{912}^G for $\gamma = [1.6, 1.4, 1.2]$ (top to bottom). In the right-hand panel, solid lines give values for $\alpha = [1.0, 2.0, 3.0]$ (bottom to top). The dashed line gives approximate values for a STARBURST99 model with continuous star formation and $Z = (1/5)Z_{\odot}$ (see text).

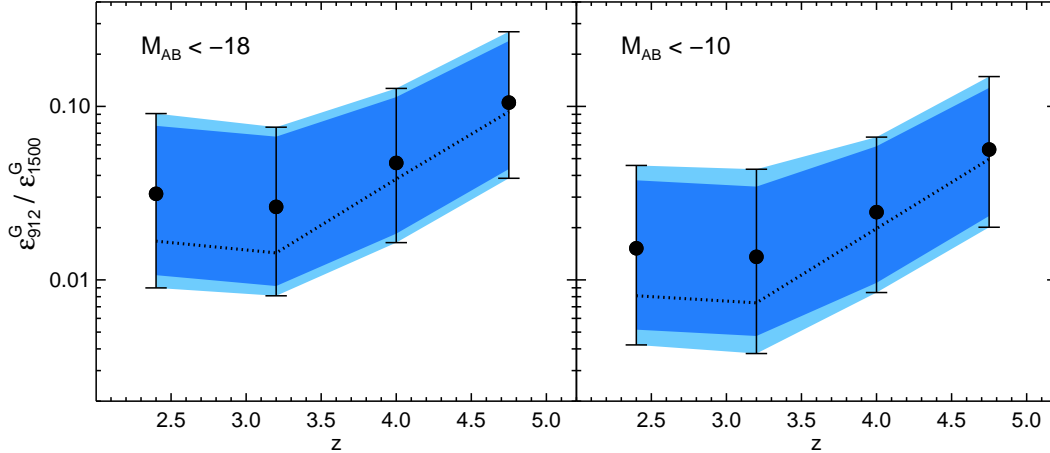


Figure 10. The ratio of ionizing to non-ionizing specific UV emissivity from galaxies, with ϵ_{1500}^G integrated down to $M_{\text{AB}} = -18$ (left-hand panel) and -10 (right-hand panel). Filled circles give our results for our fiducial parameters ($\gamma = 1.4$, $\alpha = 2.0$). The inner shaded band gives the total range of systematic uncertainty, while the outer shaded band gives the total statistical error. The dotted lines show the fiducial results when ϵ_{912}^G is calculated by subtracting the AGN emissivity from Haardt & Madau (2012).

break galaxies (LBGs) and narrow band-selected Ly α emitters (LAEs). Both studies find the ratio of ionizing to non-ionizing UV luminosity to be higher for LAEs than for LBGs. The ratio for an individual galaxy will depend on a variety of factors, including the underlying stellar population and the degree to which star-forming regions are enshrouded in neutral gas, and may not correlate perfectly with Ly α emission. Nevertheless, we can use the results of these studies to get a rough estimate of the integrated ionizing emissivity from star-forming galaxies at $z \sim 3$. Similar calculations were performed by Nestor et al. (2013) and Mostardi et al. (2013), although the ones presented here will use slightly different assumptions. For simplicity, we will primarily adopt the measurements of Nestor et al. (2013), who find $L_{912}/L_{1500} = 0.056^{+0.039}_{-0.037}$ for LBGs and $L_{912}/L_{1500} = 0.27^{+0.011}_{-0.011}$ for LAEs (inverting their η values).

The values from Mostardi et al. (2013) are lower, although consistent within the error bars.

Nestor et al. (2013) find that ~ 23 per cent of the LBGs in their sample are LAEs (Ly α rest equivalent width $\gtrsim 20 \text{ \AA}$), consistent with previous estimates at $z \sim 3$ (Steidel et al. 2000; Shapley et al. 2003; Kornei et al. 2010). This value is also consistent with trends over $4 < z < 6$ identified by Stark et al. (2011). We can obtain a lower limit on the emissivity from star-forming galaxies by integrating over the Reddy & Steidel (2009) rest-frame $\sim 1500 \text{ \AA}$ LBG luminosity function down to $M_{\text{AB}} = -18$ (roughly the observational limit), assuming that 23 per cent of LBGs are LAEs. This gives $\epsilon_{912}^{\text{SFG}} = (19.4^{+7.4}_{-7.2}) \times 10^{23} \text{ erg s}^{-1} \text{ Hz}^{-1} \text{ Mpc}^{-3}$, where we have included the uncertainty in the UV luminosity function as described in Section 6. We have so far neglected a possible luminosity dependence of Ly α emission (Stark et al. 2010, 2011), but we note that if we assume

that zero per cent of LBGs brighter than $M = -20.25$ (the bright sample of Stark et al. (2011)) are LAEs, then the above value for $\epsilon_{912}^{\text{SFG}}$ would only decrease by 16 per cent. If we integrate down to $M_{\text{AB}} = -10$ and assume that 23 per cent of LBGs are LAEs at all luminosities, then we find $\epsilon_{912}^{\text{SFG}} = (38.1_{-15.8}^{+18.4}) \times 10^{23} \text{ erg s}^{-1} \text{ Hz}^{-1} \text{ Mpc}^{-3}$. A reasonable upper limit can be obtained by instead assuming that all LBGs fainter than $M_{\text{AB}} = -18$ are LAEs, in which case $\epsilon_{912}^{\text{SFG}} = (67.7_{-31.7}^{+37.1}) \times 10^{23} \text{ erg s}^{-1} \text{ Hz}^{-1} \text{ Mpc}^{-3}$. This value becomes $\epsilon_{912}^{\text{SFG}} = (33.8_{-15.9}^{+34.7}) \times 10^{23} \text{ erg s}^{-1} \text{ Hz}^{-1} \text{ Mpc}^{-3}$ if we adopt the ionizing to non-ionizing UV luminosity ratios from Mostardi et al. (2013). We plot the extremes of these emissivity values within the 68 per cent error ranges in Figure 7, noting that the lower limit on $\epsilon_{912}^{\text{SFG}}$ is highly conservative as it neglects any contribution from galaxies fainter than $\sim 0.1L^*$. The overlap with our indirect estimate of the total emissivity from galaxies is very good, indicating that star-forming galaxies can indeed provide the majority of ionizing photons in the IGM at $z \sim 3$.

7.2 Redshift evolution in the ionizing efficiency of galaxies

Our results for $\epsilon_{912}^{\text{G}}/\epsilon_{1500}^{\text{G}}$ suggest that the luminosity-weighted ionizing “efficiency” of galaxies may be increasing with redshift from $z \sim 2 - 3$ to $z \sim 5$ (Figure 10). We reiterate that while our measurement of $\epsilon_{912}^{\text{G}}$ includes ionizing photons from all galaxies, the non-ionizing galaxy emissivity is only directly measured from galaxies brighter than $M_{\text{AB}} \simeq -18$. The apparent increase in $\epsilon_{912}^{\text{G}}/\epsilon_{1500}^{\text{G}}$ from $z = 3.2$ to $z = 4.75$ could therefore be partially negated if the relative contribution to $\epsilon_{1500}^{\text{G}}$ from fainter galaxies increases in a way not captured by the measured UV luminosity functions. The faint end slope of the UV luminosity function down to $M_{\text{AB}} = -18$ has been found to remain nearly constant over this redshift interval, so such a trend would require that the luminosity functions deviate substantially from Schechter functions at fainter luminosities. No such departure has been seen down to $M_{\text{AB}} = -13$ in observations of lensed galaxies at $z \sim 2$ (Alavi et al. 2013). The shape of the luminosity function for faint sources could be different at higher redshifts; however, at face value there appears to be a real evolution in the efficiency with which galaxies produce and/or emit ionizing photons relative to their total non-ionizing UV output.

Other trends in the properties of LBGs consistent with such an evolution have been noted. Shapley et al. (2003) and Jones et al. (2012) find a trend of decreasing absorption from low-ionization metals with increasing Ly α equivalent width in LBGs at $z \sim 3 - 4$. The decrease in absorption from low-ionization metals appears to be driven by a decrease in H I covering fraction (Jones et al. 2013), consistent with the correlation of Ly α emission and ionizing flux found by Nestor et al. (2013). Together with the observation from Stark et al. (2010, 2011) that the fraction of Ly α emitters among LBGs becomes larger with redshift over $4 < z < 6$, these trends suggests that the integrated ratio of ionizing to non-ionizing flux from LBGs should indeed be increasing with redshift, as we find.

We note that our values of $\epsilon_{912}^{\text{G}}/\epsilon_{1500}^{\text{G}}$ do not necessarily require implausibly high escape fractions of ionizing pho-

tons. The STARBURST99 model mentioned above, which had $t_{\text{age}} = 500$ Myr, constant star formation rate, and $Z = (1/5)Z_{\odot}$, has an intrinsic luminosity ratio of $L_{\nu}^{912}/L_{\nu}^{1500} \simeq 0.15$. For our fiducial value of γ , such a spectrum would have $\epsilon_{912}^{\text{G}}/\epsilon_{1500}^{\text{G}} = 0.045$ at $z = 4.75$ when integrating $\epsilon_{1500}^{\text{G}}$ down to $M_{\text{AB}} = -10$. The luminosity-weighted mean relative escape fraction would thus be $f_{\text{esc}}^{912}/f_{\text{esc}}^{1500} \simeq 0.30$. However, a BPASS model stellar population (Eldridge & Stanway 2012) with the same parameters but including massive binaries and quasi-homogeneous evolution of rapidly rotating stars has a similar shape in the ionizing region of the spectrum as the STARBURST99 model but a larger intrinsic luminosity ratio, $L_{\nu}^{912}/L_{\nu}^{1500} \simeq 0.29$. In this case the mean relative escape fraction would be $f_{\text{esc}}^{912}/f_{\text{esc}}^{1500} \simeq 0.16$, and somewhat lower if γ is less than our fiducial value.

7.3 Implications for Hydrogen Reionization

The analysis above provides at least two insights relevant to hydrogen reionization. First, the redshift evolution in $\epsilon_{912}^{\text{G}}/\epsilon_{1500}^{\text{G}}$ indicates that, for a given non-ionizing emissivity, galaxies at $z \sim 5$ emit more ionizing photons than their $z \sim 2 - 3$ counterparts. Even if this trend flattens at $z > 5$, this suggests that the galaxies responsible for hydrogen reionization produce and/or emit ionizing photons more “efficiently”, in a luminosity-weighted sense, than more well-studied galaxies at lower redshifts. Reionization models based on observed UV luminosity functions at $z > 6$ have generally concluded that such an enhanced efficiency is required for galaxies to complete reionization by $z = 6$, and have often invoked a high escape fraction for reionization-era galaxies (e.g., Ouchi et al. 2009; Kuhlen & Faucher-Giguère 2012; Mitra et al. 2013; Robertson et al. 2013). Here we present empirical evidence that such a high efficiency, whether due to a changing escape fraction or a combination of factors, is well motivated by long-term trends in $\epsilon_{912}^{\text{G}}/\epsilon_{1500}^{\text{G}}$ observed in the post-reionization epoch. We note that our fiducial increase in $\epsilon_{912}^{\text{G}}/\epsilon_{1500}^{\text{G}}$ of a factor of ~ 4 from $z = 3.2$ to 4.75 is of similar magnitude to the increase in the escape fraction adopted by Haardt & Madau (2012), who assume a factor of ~ 3 increase over the same redshift interval.

Second, the ionizing emissivity at $z \sim 4 - 5$ is around a factor of two larger than previous measurements have indicated. At $z = 4.75$, we find $\dot{N}_{\text{ion}} = 2$ to 14 ionizing photons per atom per gigayear. This higher emissivity, if it extends much beyond $z \sim 5$ (but see Bolton & Haehnelt (2007)), would make it easier to explain how the last and potentially densest 10 percent of the IGM is ionized in the 170 million years between $z = 7$ and $z = 6$ (Mortlock et al. 2011; Bolton et al. 2011), alleviating the tension between this measurement and constraints on the reionization history from independent observational probes (e.g., Ciardi et al. 2012; Jensen et al. 2013).

7.4 The Evolution of the UV background at $z > 5$

Finally, we turn towards comparing our results for the UV background to measurements at $z > 5$. Similar to previous works, we find that the H I ionization rate remains fairly flat over $2.4 \leq z \leq 4.75$. In contrast, Γ has been found to be substantially lower at $z \sim 6$ based on measurements using both the mean Ly α opacity (Bolton & Haehnelt

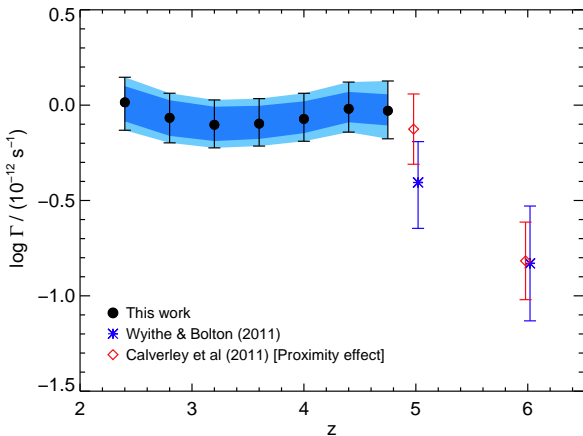


Figure 11. The evolution in the H I ionization rate over $2 < z < 6$. Circles with error bars are the present results, with systematic and statistical uncertainties given by the inner and outer shaded regions, respectively. Literature values at $z \geq 5$ are from Wyithe & Bolton (2011) (asterisks) and Calverley et al. (2011) (diamonds).

2007; Wyithe & Bolton 2011) and the quasar proximity effect (Calverley et al. 2011). We plot the redshift evolution of Γ over $2 < z < 6$ in Figure 11, where we have slightly adjusted the Wyithe & Bolton (2011) results to be consistent with our fiducial value of $\gamma = 1.4$ using the scaling from Bolton & Haehnelt (2007). Comparing our results at $z = 4.75$ to the weighted average of the literature results at $z = 6$, Γ appears to increase by 0.8 ± 0.3 dex over $\Delta z \sim 1$.

As discussed above, a change in Γ may be due to a change either in the ionizing emissivity or in the opacity of the IGM to ionizing photons (i.e., the mean free path). The fact that ϵ_{912} remains roughly constant over $2 < z < 5$, and may even increase with redshift over $3 < z < 5$, suggests that a factor of $\gtrsim 4$ decrease in the ionizing emissivity from $z \sim 5$ to $z \sim 6$ is unlikely. The non-ionizing galaxy UV emissivity, integrated down to $M_{AB} = -10$, decreases by at most a factor of 1.6 (Robertson et al. 2013). This admittedly assumes that the luminosity function remains Schechter-like over the entire faint end. At face value, however, unless the ratio of ionizing to non-ionizing emissivity decreases with redshift over $5 < z < 6$, a trend contrary that found over $3 < z < 5$, this supports the conclusion that the decline in Γ is unlikely to be driven solely by a decrease in the ionizing emissivity. The rapid evolution in the UV background over $5 < z < 6$ may therefore indicate a substantial change in the mean free path. Extrapolating our fit to the effective H I column density distribution over $2 < z < 5$, we would expect a factor of ~ 2 decline in λ_{912} between $z = 5$ and 6. A break in the mean free path evolution would therefore be required to explain the decline in Γ if the emissivity remained constant or increased with redshifts. Such a deviation in the evolution of λ_{912} may already be evident in the $z \simeq 5.1$ measurement of Worseck et al. (in prep), which was not included in our fit to $f(N_{\text{HI}}, z)$ because it is outside the redshift range of our analysis (see Figure 3). A factor of two decrease in λ_{912} coupled with a decline in ϵ_{912} proportional to that in $\epsilon_{1500}^{\text{G}}$ would also marginally be able to explain the drop in Γ .

A rapid evolution in the mean free path over $5 <$

$z < 6$, if present, would be consistent with expectations for the ‘post-overlap’ phase of reionization. As pointed out by Miralda-Escudé et al. (2000) and Furlanetto & Oh (2005), once the IGM is essentially fully ionized, the evolution in Γ is driven by the photo-evaporation of optically thick Lyman-limit systems, which largely regulate the mean free path. If such a process is occurring over $5 < z < 6$, then this would be consistent with a picture in which the overlap phase of reionization ends not long before $z \sim 6$, as suggested by the $\gtrsim 10$ percent neutral fraction measured around the $z = 7.1$ quasar ULAS J1120+0641 (Mortlock et al. 2011; Bolton et al. 2011). On the other hand, McQuinn et al. (2011) have noted that a small change in the ionizing emissivity can potentially produce a large change in Γ , particularly at $z \sim 5 - 6$, due to the coupling between Γ , ϵ_{912} , and λ_{912} . The increase in Γ from $z \sim 6$ to 5 could therefore simply reflect a modest increase in ϵ_{912} over this interval, consistent with the observed evolution in $\epsilon_{1500}^{\text{G}}$, although other factors would be required to explain why Γ then remains essentially flat over $2 < z < 5$.

Finally, we caution here that Γ at $z = 6$ may be underestimated if there is significant scatter in the intensity of the UVB at this redshift. Bolton & Haehnelt (2007) note that the photoionization rate may be underestimated by up to 10 per cent at $z \sim 6$ due to the influence of UVB fluctuations, although they incorporate this uncertainty into their published Γ measurements. Mesinger & Furlanetto (2009) also note UVB fluctuations will alter the inferred photoionization rates by a few per cent at these redshifts.

8 SUMMARY

We have presented new measurements of the intensity of the UV background and the global ionizing emissivity over $2 < z < 5$. The results are based on recent measurements of the mean Ly α opacity and temperature of the IGM, as well as the opacity of the IGM to ionizing photons. This study benefits from the precision of these new measurements, as well as from the fact that the measurements are self-consistent over a wide redshift range.

Similar to previous works (e.g., Bolton et al. 2005; Bolton & Haehnelt 2007; Faucher-Giguère et al. 2008a), we find that the hydrogen photoionization rate, Γ , stays roughly constant over $2 < z < 5$. We find a factor of two larger Γ than that obtained by Faucher-Giguère et al. (2008a), however, a difference due mainly to our lower IGM temperatures. Our results for the ionizing emissivity are also considerably higher than previous estimates (Bolton & Haehnelt 2007; Kuhlen & Faucher-Giguère 2012). This is due to a combination of lower IGM temperatures, a higher opacity to ionizing photons, and the fact that our calculations take into account cosmological radiative transfer effects.

We calculate the emissivity of star-forming galaxies by subtracting estimates for the emissivity of AGN made by Cowie et al. (2009) from our total emissivity measurements. We find that galaxies dominate the UV background near 1 Ryd, especially at $z \geq 4$, and that $\epsilon_{912}^{\text{G}}$ may increase with redshift over this interval. Our estimate for $\epsilon_{912}^{\text{G}}$ is consistent with estimates of the emissivity from star-forming galaxies at $z \sim 3$ based on direct measurements of the ionizing output from Lyman break galaxies and Ly α emitters (Nestor et al.

2013; Mostardi et al. 2013). Comparing ϵ_{912}^G to the non-ionizing UV emissivity of galaxies over $2 < z < 5$ determined from rest-frame UV luminosity functions (Reddy & Steidel 2009; Bouwens et al. 2007), we find that the ionizing “efficiency” of galaxies remains relatively flat over $2.4 \leq z \leq 3.2$ but may increase substantially from $z = 3.2$ to $z = 4.75$. Assuming that the faint end of the luminosity function over this interval is well described by the measured Schechter functions, the ratio of ionizing to non-ionizing emissivity would remain flat only if the ionizing source spectrum near 912 \AA softened dramatically from $z \sim 5$ to $z \sim 3$. We note that the increase in $\epsilon_{912}^G/\epsilon_{1500}^G$ with redshift would become even stronger if we used the higher AGN emissivity adopted by Haardt & Madau (2012), which is based on the AGN luminosity functions of Hopkins et al. (2007).

Our results carry multiple implications for hydrogen reionization. First, we have shown that the ionizing efficiency of galaxies appears to increase with redshift in the post-reionization epoch. This evolution supports the conclusion often drawn from reionization modeling that reionization-era galaxies must produce and/or emit ionizing photons significantly more efficiently than their lower-redshift counterparts in order to complete reionization by $z = 6$ (e.g., Ouchi et al. 2009; Kuhlen & Faucher-Giguère 2012; Mitra et al. 2013; Robertson et al. 2013). Second, we find that ionizing photons appear to be a factor of two more abundant in the IGM at $z \sim 5$ compared to previous studies, with $\dot{N}_{\text{ion}} \simeq 2 - 14$ ionizing photons/atom/gigayear ($\dot{N}_{\text{ion}} \sim 5$ photons/atom/gigayear for realistic galaxy spectra). This high emissivity, if it persists to higher redshifts, would explain how the last, and potentially densest, 10 per cent of the IGM may have been reionized after $z = 7$ (Mortlock et al. 2011; Bolton et al. 2011).

Finally, the relatively flat ionization rate we find over $2.4 \leq z \leq 4.75$ contrasts with the sharp decline measured from $z \sim 5$ to 6. The low measurement of Γ at $z \sim 6$ has previously been interpreted as evidence for a low ionizing emissivity and a “photon-starved” mode of reionization (Bolton & Haehnelt 2007; Calverley et al. 2011). In light of the fact that the emissivity we measure appears to remain flat or increase with redshift over $3 < z < 5$, the decrease in Γ may instead signify a rapid evolution in the mean free path, consistent with the photoionization of Lyman limit systems at the end of the ‘post-overlap’ phase of reionization (e.g., Furlanetto & Oh 2005, but see McQuinn et al. 2011). Under this scenario, ionizing photons may have been considerably more abundant during the final stages of reionization than has previously been recognized.

ACKNOWLEDGEMENTS

We are extremely grateful to Michele Fumagalli and Gabor Worseck, who allowed us to use their mean free path measurements ahead of publication. We are also grateful to John Eldridge, Martin Haehnelt, John O’Meara, Xavier Prochaska, and Naveen Reddy for helpful conversations. We thank Volker Springel for making GADGET-3 available. We also thank the anonymous referee for helpful comments. The hydrodynamical simulations used in this work were performed using the Darwin Supercomputer of the University of Cambridge High Performance Computing Service

(<http://www.hpc.cam.ac.uk/>), provided by Dell Inc. using Strategic Research Infrastructure Funding from the Higher Education Funding Council for England. GDB gratefully acknowledges support from the Kavli Foundation. JSB acknowledges the support of a Royal Society University Research Fellowship.

REFERENCES

- Alavi, A., et al. 2013, arXiv:1305.2413
 Bajtlik, S., Duncan, R. C., & Ostriker, J. P. 1988, *ApJ*, 327, 570
 Becker, G. D., Bolton, J. S., Haehnelt, M. G., & Sargent, W. L. W. 2011, *MNRAS*, 410, 1096
 Becker, G. D., Hewett, P. C., Worseck, G., & Prochaska, J. X. 2013, *MNRAS*, 430, 2067
 Bolton, J., Meiksin, A., & White, M. 2004, *MNRAS*, 348, L43
 Bolton, J. S., & Becker, G. D. 2009, *MNRAS*, 398, L26
 Bolton, J. S., & Haehnelt, M. G. 2007, *MNRAS*, 382, 325
 Bolton, J. S., Haehnelt, M. G., Viel, M., & Springel, V. 2005, *MNRAS*, 357, 1178
 Bolton, J. S., Haehnelt, M. G., Warren, S. J., Hewett, P. C., Mortlock, D. J., Venemans, B. P., McMahon, R. G., & Simpson, C. 2011, *MNRAS*, 416, L70
 Bolton, J. S., Viel, M., Kim, T.-S., Haehnelt, M. G., & Carswell, R. F. 2008, *MNRAS*, 386, 1131
 Bouwens, R., et al. 2012, arXiv:1211.2230
 Bouwens, R. J., Illingworth, G. D., Blakeslee, J. P., & Franx, M. 2006, *ApJ*, 653, 53
 Bouwens, R. J., Illingworth, G. D., Franx, M., & Ford, H. 2007, *ApJ*, 670, 928
 —. 2008, *ApJ*, 686, 230
 Bouwens, R. J., et al. 2011, *ApJ*, 737, 90
 Bunker, A. J., et al. 2010, *MNRAS*, 409, 855
 Calverley, A. P., Becker, G. D., Haehnelt, M. G., & Bolton, J. S. 2011, *MNRAS*, 412, 2543
 Castellano, M., et al. 2010, *A&A*, 524, 28
 Ciardi, B., Bolton, J. S., Maselli, A., & Graziani, L. 2012, *MNRAS*, 423, 558
 Compostella, M., Cantalupo, S., & Porciani, C. 2013, arXiv:1306.5745
 Cowie, L. L., Barger, A. J., & Trouille, L. 2009, *ApJ*, 692, 1476
 Dall’Aglio, A., Wisotzki, L., & Worseck, G. 2008, *A&A*, 491, 465
 Eldridge, J. J., & Stanway, E. R. 2012, *MNRAS*, 419, 479
 Ellis, R. S., et al. 2013, *ApJ*, 763, L7
 Fan, X., et al. 2006, *AJ*, 132, 117
 Fardal, M. A., Giroux, M. L., & Shull, J. M. 1998, *ApJ*, 115, 2206
 Faucher-Giguère, C.-A., Lidz, A., Hernquist, L., & Zaldarriaga, M. 2008a, *ApJ*, 688, 85
 Faucher-Giguère, C.-A., Lidz, A., Zaldarriaga, M., & Hernquist, L. 2009, *ApJ*, 703, 1416
 Faucher-Giguère, C.-A., Prochaska, J. X., Lidz, A., Hernquist, L., & Zaldarriaga, M. 2008b, *ApJ*, 681, 831
 Ferrara, A., & Loeb, A. 2013, *MNRAS*, 431, 2826
 Fontanot, F., Cristiani, S., & Vanzella, E. 2012, *MNRAS*, 425, 1413

- Fumagalli, M., O’Meara, J. M., Prochaska, J. X., & Worseck, G. 2013, arXiv:1308.1101
- Furlanetto, S. R., & Oh, S. P. 2005, MNRAS, 363, 1031
- . 2009, ApJ, 701, 94
- Gunn, J. E., & Peterson, B. A. 1965, ApJ, 142, 1633
- Haardt, F., & Madau, P. 1996, ApJ, 461, 20
- . 2012, ApJ, 746, 125
- Hopkins, P. F., Richards, G. T., & Hernquist, L. 2007, ApJ, 654, 731
- Hui, L., & Gnedin, N. Y. 1997, MNRAS, 292, 27
- Jena, T., et al. 2005, MNRAS, 361, 70
- Jensen, H., Laursen, P., Mellema, G., Iliev, I. T., Sommer-Larsen, J., & Shapiro, P. R. 2013, MNRAS, 428, 1366
- Jones, T., Ellis, R. S., Schenker, M. A., & Stark, D. P. 2013, arXiv:1304.7015
- Jones, T., Stark, D. P., & Ellis, R. S. 2012, ApJ, 751, 51
- Kirkman, D., et al. 2005, MNRAS, 360, 1373
- Kornei, K. A., Shapley, A. E., Erb, D. K., Steidel, C. C., Reddy, N. A., Pettini, M., & Bogosavljević, M. 2010, ApJ, 711, 693
- Kuhlen, M., & Faucher-Giguère, C.-A. 2012, MNRAS, 423, 862
- Lee, K.-G. 2012, ApJ, 753, 136
- Leitherer, C., et al. 1999, ApJS, 123, 3
- Madau, P., Haardt, F., & Rees, M. J. 1999, ApJ, 514, 648
- McDonald, P., & Miralda-Escudé, J. 2001, ApJ, 549, L11
- McLure, R. J., Dunlop, J. S., Cirasuolo, M., Koekemoer, A. M., Sabbi, E., Stark, D. P., Targett, T. A., & Ellis, R. S. 2010, MNRAS, 403, 960
- McLure, R. J., et al. 2013, MNRAS, 1319
- McQuinn, M., Lidz, A., Zaldarriaga, M., Hernquist, L., Hopkins, P. F., Dutta, S., & Faucher-Giguère, C.-A. 2009, ApJ, 694, 842
- McQuinn, M., Oh, S. P., & Faucher-Giguère, C.-A. 2011, ApJ, 743, 82
- Meiksin, A. 2005, MNRAS, 356, 596
- Meiksin, A., & Tittley, E. R. 2012, MNRAS, 423, 7
- Meiksin, A., & White, M. 2003, MNRAS, 342, 1205
- Mesinger, A., & Furlanetto, S. 2009, MNRAS, 400, 1461
- Miralda-Escudé, J. 2003, ApJ, 597, 66
- Miralda-Escudé, J., Haehnelt, M., & Rees, M. J. 2000, ApJ, 530, 1
- Mitra, S., Ferrara, A., & Choudhury, T. R. 2013, MNRAS, 428, L1
- Mortlock, D. J., et al. 2011, Nature, 474, 616
- Mostardi, R. E., Shapley, A. E., Nestor, D. B., Steidel, C. C., & Reddy, N. A. 2013, arXiv:1306.1535
- Nestor, D. B., Shapley, A. E., Kornei, K. A., Steidel, C. C., & Siana, B. 2013, ApJ, 765, 47
- Oesch, P. A., et al. 2010, ApJ, 709, L16
- O’Meara, J. M., Prochaska, J. X., Burles, S., Prochter, G., Bernstein, R. A., & Burgess, K. M. 2007, ApJ, 656, 666
- O’Meara, J. M., Prochaska, J. X., Worseck, G., Chen, H.-W., & Madau, P. 2013, ApJ, 765, 137
- Osterbrock, D. E., & Ferland, G. J. 2006, Astrophysics of gaseous nebulae and active galactic nuclei, Second Edition. Sausalito: University Science Books, pp. 20
- Ouchi, M., et al. 2009, ApJ, 706, 1136
- . 2010, ApJ, 723, 869
- Paresce, F., McKee, C. F., & Bowyer, S. 1980, ApJ, 240, 387
- Pawlik, A. H., Schaye, J., & van Scherpenzeel, E. 2009, MNRAS, 394, 1812
- Péroux, C., McMahon, R. G., Storrie-Lombardi, L. J., & Irwin, M. J. 2003, MNRAS, 346, 1103
- Planck Collaboration XVI 2013, arXiv:1303.5076
- Prochaska, J. X., O’Meara, J. M., & Worseck, G. 2010, ApJ, 718, 392
- Prochaska, J. X., Worseck, G., & O’Meara, J. M. 2009, ApJ, 705, L113
- Rauch, M., et al. 1997, ApJ, 489, 7
- Reddy, N. A., & Steidel, C. C. 2009, ApJ, 692, 778
- Robertson, B. E., et al. 2013, ApJ, 768, 71
- Rollinde, E., Theuns, T., Schaye, J., Pâris, I., & Petitjean, P. 2013, MNRAS, 428, 540
- Rudie, G. C., Steidel, C. C., & Pettini, M. 2012, ApJ, 757, L30
- Schenker, M. A., et al. 2013, ApJ, 768, 196
- Schirber, M., & Bullock, J. S. 2003, ApJ, 584, 110
- Scott, J., Bechtold, J., Dobrzycki, A., & Kulkarni, V. P. 2000, ApJS, 130, 67
- Shapley, A. E., Steidel, C. C., Pettini, M., & Adelberger, K. L. 2003, ApJ, 588, 65
- Siana, B., et al. 2010, ApJ, 723, 241
- Songaila, A., & Cowie, L. L. 2010, ApJ, 721, 1448
- Songaila, A., Hu, E. M., Cowie, L. L., & McMahon, R. G. 1999, ApJ, 525, L5
- Springel, V. 2005, MNRAS, 364, 1105
- Stark, D. P., Ellis, R. S., Chiu, K., Ouchi, M., & Bunker, A. 2010, MNRAS, 408, 1628
- Stark, D. P., Ellis, R. S., & Ouchi, M. 2011, ApJ, 728, L2
- Steidel, C. C., Adelberger, K. L., Shapley, A. E., Pettini, M., Dickinson, M., & Giavalisco, M. 2000, ApJ, 532, 170
- Telfer, R. C., Zheng, W., Kriss, G. A., & Davidsen, A. F. 2002, ApJ, 565, 773
- Theuns, T., Leonard, A., Efstathiou, G., Pearce, F. R., & Thomas, P. A. 1998, MNRAS, 301, 478
- Trac, H., Cen, R., & Loeb, A. 2008, ApJ, 689, L81
- Tytler, D., et al. 2004, ApJ, 617, 1
- Viel, M., Bolton, J. S., & Haehnelt, M. G. 2009, MNRAS, 399, L39
- Wyithe, J. S. B., & Bolton, J. S. 2011, MNRAS, 412, 1926
- York, D. G., et al. 2000, AJ, 120, 1579
- Zaldarriaga, M., Hui, L., & Tegmark, M. 2001, ApJ, 557, 519

APPENDIX A: SCALING RELATIONS FOR Γ

Here we update the scaling relations from Bolton et al. (2005) and Bolton & Haehnelt (2007) describing the dependence of the photoionization rate on the effective optical depths and the parameters of the temperature-density relation. For the effective optical depth, power law relations of the form $\Gamma \propto (\tau_{\text{eff}}^{\alpha})^{x_{\alpha}}$ were empirically determined as a function of redshift from the simulations. These were found to describe the dependence of Γ on $\tau_{\text{eff}}^{\alpha}$ very accurately, with x_{α} decreasing from -1.46 at $z = 1.998$ to -1.78 at $z = 4.915$ (Figure A1), similar to the results of Bolton et al. (2005) and Bolton & Haehnelt (2007)

In order to assess the scaling of Γ with gas temperature, we imposed power law temperature-density relations

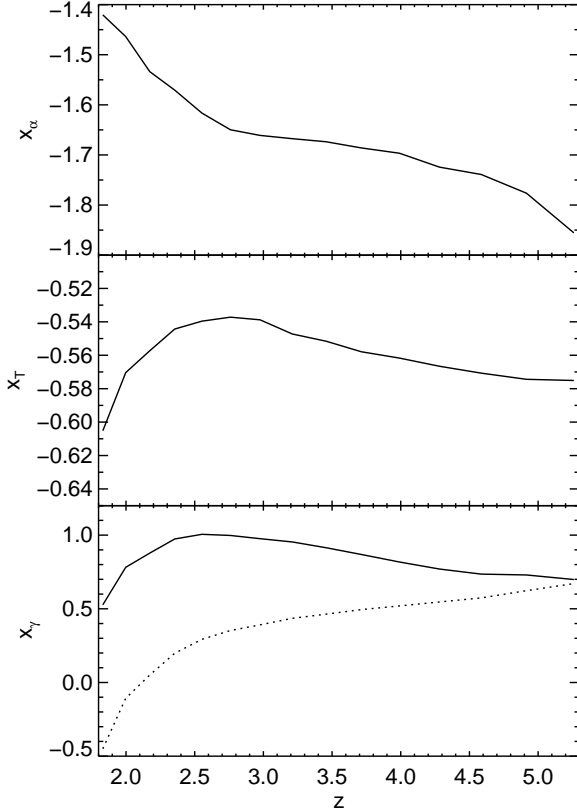


Figure A1. Scaling coefficients for Γ as a function of redshift. x_α (upper panel) and x_T (middle panel) are the power law indices for the scaling of Γ with τ_{eff}^α and $T(\bar{\Delta})$, respectively. x_γ (lower panel) is the exponential coefficient for the scaling of Γ with γ in the cases where $T(\bar{\Delta})$ and T_0 are held fixed (solid and dotted lines, respectively).

of the form $T(\Delta) = \bar{T}(\Delta/\bar{\Delta})^{\gamma-1}$ on our fiducial simulation, and separately evaluated the dependence of Γ on $T(\bar{\Delta})$ and γ . When changing the gas temperature, the hydrogen neutral fraction was also scaled as $f_{\text{HI}} \propto T^{-0.72}$. Changes in Γ with $T(\bar{\Delta})$ were found to be well described by power laws of the form $\Gamma \propto \bar{T}^{x_T}$, with $x_T \simeq 0.55$ but varying slightly with redshift (Figure A1). This scaling is similar to the results obtained by Bolton et al. (2005) and Bolton & Haehnelt (2007). The slightly weaker dependence of Γ on $T(\bar{\Delta})$ compared to what one would expect from equation (2) reflects the fact that the decrease in τ_{eff}^α with Γ due to the decrease in the recombination rate is somewhat offset by an increase in τ_{eff}^α due to increased thermal broadening.

We evaluated the dependence of Γ on the slope of the temperature-density relation by varying γ while holding $T(\bar{\Delta})$ fixed. The result was an exponential scaling of the form $\Gamma \propto \exp(x_\gamma \gamma)$, with x_γ varying with redshift between 0.76 and 1.00 (Figure A1). This is a stronger dependence on γ than if the temperature was always held fixed at the mean density, the results for which we also plot in Figure A1. This difference is simply due to the fact that τ_{eff}^α is mainly sensitive to the opacity of the voids. We note that Γ becomes largely insensitive to γ if the temperature is known near $\Delta \sim 0.5$ (although the precise value of Δ depends on the redshift). In principle, this means that if Γ can

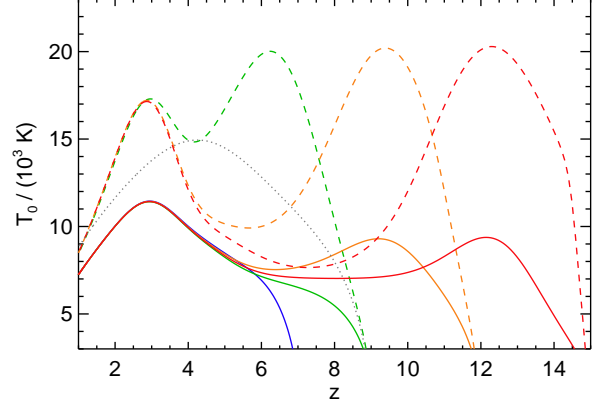


Figure B1. Thermal histories for the hydrodynamical simulations used in this work. Temperatures at the mean density are plotted as a function of redshift. The solid and dashed lines show runs used to assess the impact of Jeans smoothing on Γ . The dotted line shows the thermal history for the C15 and R runs.

be accurately measured by some other method, such as the proximity effect, it may be possible to infer a value for γ .

APPENDIX B: IMPACT OF JEANS SMOOTHING

In addition to the role of gas temperature in setting the H I recombination rate and the thermal broadening of absorption lines, the integrated thermal history of the IGM can potentially affect our estimate of Γ through its impact on the baryon density distribution. On large scales the baryons will generally trace the underlying dark matter, whose density field can be predicted from cosmology. On small scales, however, the baryon distribution will be smoothed due to thermal pressure. This effect, known as ‘‘Jeans smoothing’’, is particularly significant during hydrogen reionization, when the temperature of the gas is increased by orders of magnitude (e.g., Pawlik et al. 2009).

To test whether Jean smoothing may impact our Γ measurements, we ran a set of simulations in which the timing and amplitude of photoionization heating during hydrogen (as well as at lower redshifts) were varied. The thermal histories for these runs are shown in Figure B1. Our fiducial values of Γ were calculated using the density and peculiar velocity fields from the run in which hydrogen reionization begins at $z = 12$ and the gas is heated to $\sim 9,000$ K by $z \simeq 9$. Using the density and peculiar velocity fields from other runs was found to have a minimal ($\lesssim 0.02$ dex) impact on Γ . Uncertainties related to Jeans smoothing are nevertheless included in our systematic error budget (Tables 1 and 3).

APPENDIX C: EMISSIVITY CALCULATION

In Section 5 we described how we compute the ionizing emissivity from the H I ionization rate and the opacity of the IGM+CGM to ionizing photons. Our calculations were based on the full equation of cosmological radiative transfer, which allowed us to take into account the redshifting of

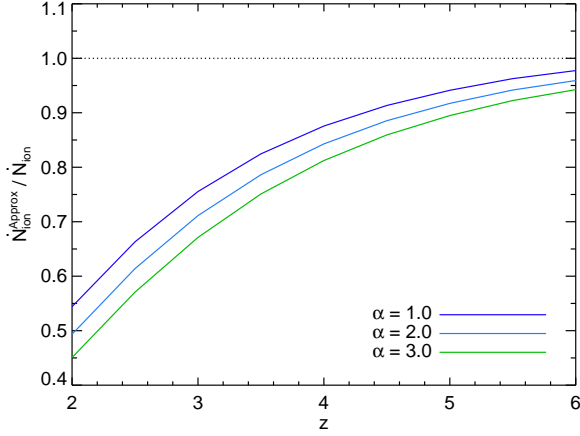


Figure C1. The ratio of the ionizing emissivity computed from the approximation given by equation (C3) to that computed using full cosmological radiative transfer. Solid lines are for $\alpha = 1.0, 2.0$ and 3.0 (top to bottom).

ionizing photons as they propagate through the IGM (e.g., Haardt & Madau 1996).

It has been common to simplify the calculation of the emissivity by assuming that the mean free path of ionizing photons is short enough to neglect the redshifting effect. Under this “local source” approximation, equation (3) reduces to (e.g., Schirber & Bullock 2003)

$$J_\nu \approx \frac{1}{4\pi} \lambda(\nu, z) \epsilon_\nu(z). \quad (\text{C1})$$

In addition, calculations of the mean free path based on the H I column density distribution (equation (5)) have also commonly used an approximate expression that neglects redshifting (i.e., $z_0 \simeq z$), such that

$$\lambda(\nu, z) \approx \frac{(\beta_N - 1)c}{\Gamma(2 - \beta_N) N_{\text{LL}} \sigma_{912}^{\beta_N - 1}} \left(\frac{\nu}{\nu_{912}} \right)^{2.75(\beta_N - 1)} \times \frac{1}{(1+z)^{\beta_z + 1} H(z)} \quad (\text{C2})$$

(e.g., Madau et al. 1999; Faucher-Giguère et al. 2008a, equation (22)), where Γ here is the gamma function.

Combining equations (1), (7) and (C1), and integrating over frequency gives (e.g., Kuhlen & Faucher-Giguère 2012)

$$\dot{N}_{\text{ion}}(z) \approx \frac{1}{(1+z)^3} \frac{\Gamma(z)}{\sigma_{912} \lambda_{912}(z)} \frac{(\alpha_{\text{bg}} + 2.75)}{\alpha}. \quad (\text{C3})$$

Here we have modeled the specific intensity as a power law in frequency, $J_\nu = J_{912}(\nu/\nu_{912})^{\alpha_{\text{bg}}}$ for $\nu \geq \nu_{912}$, where for a power-law distribution of H I column densities, $f(N_{\text{HI}}) \propto N_{\text{HI}}^{-\beta_N}$, the slope of the ionizing background is given by $\alpha_{\text{bg}} = \alpha - 2.75(\beta_N - 1)$.

In Figure C1 we plot the approximate value of \dot{N}_{ion} given by equations (C2) and (C3) as a fraction of the value obtained from the full calculation described in Section 5. For this comparison we assume that Γ is constant with redshift, and adopt our nominal H I column density distribution parameters $[A, \beta_N, \beta_z] = [0.93, 1.33, 1.92]$. The approximate expression for \dot{N}_{ion} asymptotically approaches the exact value with increasing redshift, with $\dot{N}_{\text{ion}}^{\text{approx}} / \dot{N}_{\text{ion}} \geq 0.8$ for $z > 3.6$ and $\alpha < 2$. At $z \sim 2 - 3$, however, the approxi-

mate expression is significantly too low, up to a factor of two at $z = 2$. This can be understood from the fact that, once the mean free path becomes sufficiently large, a significant fraction of ionizing photons will redshift beyond the Lyman limit before they are absorbed. The approximate expression for \dot{N}_{ion} neglects this effect, and so requires a lower emissivity for a given ionization rate. The effect is greater for softer ionizing spectra, where a larger fraction of the ionizing flux is concentrated near the Lyman limit. Even for $\alpha = 1.0$, however, the approximate calculation delivers a value for \dot{N}_{ion} that is significantly too low at $z < 4$.

Finally, we emphasize that the results plotted in Figure C1 apply only when the approximate expressions for both λ_{912} and \dot{N}_{ion} are used. If equation C3 is instead evaluated using the exact λ_{912} values calculated from $f(N_{\text{HI}}, z)$ as described in Section 5.1, or measured directly from composite spectra (Prochaska et al. 2009; O’Meara et al. 2013; Fumagalli et al. 2013, Worseck et al., in prep), the emissivity will be underestimated by an even greater factor.